

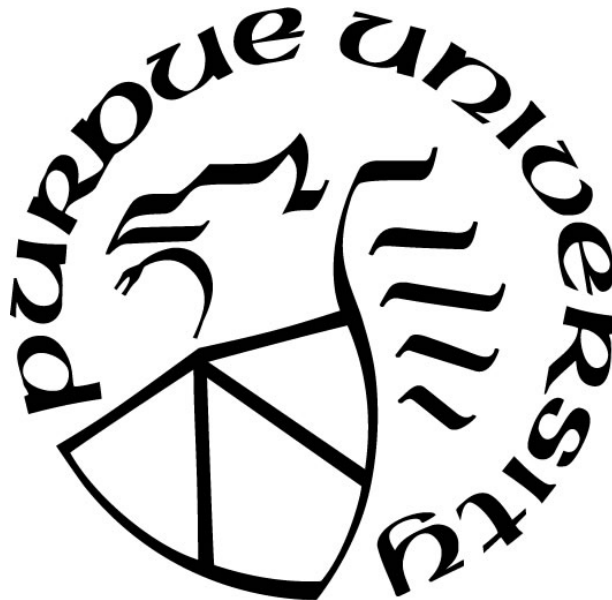
**AN ITERATIVE PROCEDURE WITH IMPROVED INITIAL GUESS TO
EVALUATE THE SEVEN PARAMETERS OF THE TWO DIODE MODEL
FOR A PHOTOVOLTAIC MODULE**

by
Ziyue Liu

A Thesis

*Submitted to the Faculty of Purdue University
In Partial Fulfillment of the Requirements for the degree of*

Master of Science in Engineering



Department of Electrical and Computer Engineering
Hammond, Indiana
December 2021

THE PURDUE UNIVERSITY GRADUATE SCHOOL
STATEMENT OF COMMITTEE APPROVAL

Dr. David Kozel, Chair

School of Engineering

Dr. Nasser Houshang

School of Engineering

Dr. Constantin Apostoia

School of Engineering

Approved by:

Dr. Xiaoli Yang

Dedicated to my advisor, parents and Haibo.

ACKNOWLEDGMENTS

I would like to thank my advisor Prof. Kozel. He gave me a lot of academic guidance and helped in the past two years. He taught me how to do research and how to write a thesis. He was very patient with me. Since I am not a native English speaker, he always asked if I understand when explaining problems to me. When revising my paper, he told me how to be more professional with the English language. He also gave me a lot of suggestions on my future path. Last year's distance learning gave everyone great challenges. I am very grateful to my advisor for his help and encouragement during such difficult times.

I would like to thank to my committee members, Prof. Constantin Apostoiaia and Prof. Nasser Houshang, for their feedback and encouragement.

I would like to thank to my parents and my fiancé Haibo. My parents have been giving me a lot of support even though we were in different countries and time zones. Even though we have not seen each other for two years, I can always feel their love for me no matter where I am. My fiancé received his Ph.D. in August this year, which inspires me a lot when conducting this research. I respect his seriousness, rigorousness, and perseverance. We spent very difficult time together during the epidemic.

Finally, I could not have completed this thesis without the support of my friends. They have brought me a lot of happiness.

TABLE OF CONTENTS

LIST OF TABLES	7
LIST OF FIGURES	8
NOMENCLATURE	10
ABSTRACT.....	11
1. INTRODUCTION	12
1.1 Background	12
1.2 Literature review	16
1.3 Objectives	20
2. METHODOLOGY	22
2.1 One diode model	22
2.1.1 Mathematic model	22
2.1.2 Characteristics of I - V and P - V curves of the single diode model	26
2.2 Double diode model	31
2.2.1 Mathematic model	31
2.2.2 Sensitivity of n_2	32
2.2.3 Sensitivity of I_{o2}	35
3. OPTIMIZATION OF MODEL PARAMETERS	38
3.1 Mathematic model	38
3.2 Newton-Raphson method.....	41
3.3 Determination of model parameters.....	43
4. RESULTS	46
4.1 Comparison with Trinasolar	46
4.1.1 Manufacturer datasheet.....	46
4.1.2 Optimized model parameter	48
4.1.3 I - V and P - V characteristics	49
4.1.4 Effect of irradiance	51
4.2 Comparison with SolarEdge	53
4.2.1 Manufacturer datasheet.....	53
4.2.2 Optimized model parameter	55

4.2.3	<i>I-V</i> and <i>P-V</i> characteristics	56
4.2.4	Effect of irradiance	58
5.	CONCLUSION.....	60
5.1	Conclusions.....	60
5.2	Future work.....	61
	REFERENCES	62

LIST OF TABLES

Table 4-1 Electrical data of the PV module TSM-PD14 (335W) [63]	48
Table 4-2 Summary of the optimized model parameters for the PV module TSM-PD14 (335W)	49
Table 4-3 Electrical data of the PV module SPV300-60MMJ [66].....	55
Table 4-4 Summary of the optimized model parameters for the PV module SPV300-60MMJ [66]	56

LIST OF FIGURES

Figure 1-1. Shares of total U.S. energy consumption by major sources in selected years (1776-2020) [3].....	13
Figure 1-2. U.S. primary energy consumption by energy source in 2020 [3]	13
Figure 1-3. U.S. electricity generation from renewable energy sources (1950-2020) [4]	14
Figure 1-4. Schematic illustration of a photovoltaic cell and its working principle [7].	15
Figure 1-5. Illustration of a photovoltaic system [9]	16
Figure 1-6. An ideal PV panel model [11].....	17
Figure 1-7. Improved single diode equivalent circuit.....	18
Figure 1-8. Extension of the improved single diode equivalent circuit [11]	18
Figure 1-9. Double diode equivalent circuit	19
Figure 2-1. An ideal PV panel model [11].....	22
Figure 2-2. Comparison of manufacture's I - V curve with the simple diode model under the irradiance of 200W/m^2	23
Figure 2-3. Effect of I_0 on the simple PV panel I - V Model for $n = 1$	24
Figure 2-4. Effect of n on the simple PV panel I - V Model for $I_0 = 1.3 \times 10^{-10}$	25
Figure 2-5. Single diode equivalent circuit [11]	26
Figure 2-6. I - V characteristic of the single diode model and ideal model	27
Figure 2-7. P - V characteristic of the single-diode model and ideal model.....	27
Figure 2-8. I - V curve in response to the change of R_p	28
Figure 2-9. P - V curve in response to the change of R_p	29
Figure 2-10. I - V curve in response to the change of R_s when $R_p = 750$	30
Figure 2-11. P - V curve in response to the change of R_s when $R_p = 750$	30
Figure 2-12. Double diode equivalent circuit	31
Figure 2-13. I - V curve in response to the change of n_2 : (a) the full range, and (b) enlarged view	33
Figure 2-14. P - V curve in response to the change of n_2 : (a) the full range, and (b) enlarged view	34
Figure 2-15. I - V curve in response to the change of I_{o2}/I_{o1} for $n_2 = 1.2$	35
Figure 2-16. P - V curve in response to the change of I_{o2}/I_{o1} for $n_2 = 1.2$	36

Figure 2-17. I - V curve in response to the change of I_{o2}/I_{o1} for $n_2 = 1.8$	37
Figure 2-18. P - V curve in response to the change of I_{o2}/I_{o1} for $n_2 = 1.8$	37
Figure 3-1. Visualization of the Newton-Raphson method	42
Figure 3-2. Flowchart of the iterative process	44
Figure 4-1. Dimensions of the PV module TSM-PD14 (mm/inch) [63]: (a) back view, and (b) cross-section A-A.....	46
Figure 4-2. I - V curves of the PV module TSM-PD14 (335W) [63]	47
Figure 4-3. P - V curves of the PV module TSM-PD14 (335W) [63]	47
Figure 4-4. Comparison between the measured I - V characteristic and the calculated characteristic in the standard test condition	50
Figure 4-5. Comparison between the measured P - V characteristic and the calculated characteristic in the standard test condition	50
Figure 4-6. U.S. annual global horizontal irradiance [65]	51
Figure 4-7. Comparison between the measured I - V characteristic of the PV module TSM-PD14 and the calculated characteristic at different irradiances	52
Figure 4-8. Comparison between the measured P - V characteristic of the PV module TSM-PD14 and the calculated characteristic at different irradiances	52
Figure 4-9. Dimensions of the PV module SPV300-60MMJ [66]: (a) front view, side view, and back view, and (b) cross-section view.	53
Figure 4-10. I - V curves of the PV module SPV300-60MMJ [66]	54
Figure 4-11. P - V curves of the PV module SPV300-60MMJ [66]	54
Figure 4-12. Comparison between the measured I - V characteristic and the calculated characteristic in the standard test condition	57
Figure 4-13. Comparison between the measured P - V characteristic and the calculated characteristic in the standard test condition	57
Figure 4-14. Comparison between the measured I - V characteristic of the PV module SPV300-60MMJ and the calculated characteristic at different irradiances	58
Figure 4-15. Comparison between the measured P - V characteristic of the PV module SPV300-60MMJ and the calculated characteristic at different irradiances	59

NOMENCLATURE

$P-V$	Power-Voltage
$I-V$	Current-Voltage
R_s	Series resistance
K_v	Open circuit voltage coefficient
R_p	Parallel (shunt) resistance
I_{sc}	Short circuit current
I_{sh}	Current passing through R_p
I_o	Saturation current
n	Diode ideality factor
I_{ph}	Photo-generated current
V_D	Voltage across the p-n junction
V_T	Thermal voltage of the PV panel
N_s	Number of PV cells
k	Boltzmann's constant
q	Electron charge
T	Temperature
I_D	Current passing through the diode
V_{OC}	Open circuit voltage
K_I	Short circuit current/temperature coefficient
G	Irradiance on the device surface
V_{mp}	Voltage at the maximum power point
I_{mp}	Current at the maximum power point
a	diode constant
P	Power
K_V	Short circuit voltage/temperature coefficient
ε_{mp}	Error at the maximum power point

ABSTRACT

Climate change and global warming indicate that reducing the use of traditional fossil energy and developing new renewable energy should be an essential matter. Solar energy has emerged as one of the renewable energy sources for electricity generation since the late 20th century. One way to utilize solar energy is to collect and convert it into electricity by solar photovoltaic devices through the photovoltaic effect. Due to the high cost of photovoltaic modules, it is essential to optimize the performance of photovoltaic modules by using accurate equivalent circuit models. Among the available equivalent circuit models, the single diode model is relatively simple and computationally efficient but would be inaccurate if the recombination loss were substantial. The double diode model includes more parameters to represent the recombination loss, so the accuracy improves, but at the cost of adding more parameters to the model. The primary challenge of applying the double diode model is obtaining the optimum value for the seven model parameters with a reasonable computational effort.

The current study investigates the effect of each term in the double diode model. It then proposes a method to obtain an initial estimate for each of the seven model parameters from data provided by the manufacturer. Using these initial estimated parameters as inputs, the Newton-Raphson method is applied to improve parameter estimates and prediction accuracy. The performance of two PV modules from different manufacturers is then modeled using the initial parameter estimates and the Newton-Raphson updated parameters. Both are compared to the manufacturers' data.

1. INTRODUCTION

1.1 Background

Making fire and burning wood were the main energy sources of the first generation of humans. Engels suggests that the subsequent major developments following from the development of the meat diet were the control of fire, and the domestication of animals [1]. Due to the rise of the Industrial Revolution, coal became the most widely used energy source in the mid-17th century. From the end of the 19th century to the middle of the 20th century, oil replaced coal as the main energy source with more advantages such as less pollution and higher energy density [2]. Since the 1930s, the drawbacks of various fossil fuels have begun to appear, and other new energy technologies have become increasingly mature and put into use [1].

Climate change and global warming indicate that reducing the use of traditional fossil energy and developing new renewable energy should be an essential matter. For example, the energy consumption in the U.S. has been shifting from fossil fuel, hydropower, and wood to biofuels, geothermal energy, solar energy, and wind energy since the beginning of the 21st century, as shown in Figure 1-1 [3]. As shown in Figure 1-2, in 2020, renewable energy provided about 11.59 quadrillion British thermal units (Btu) out of the 92.94 quadrillion Btu energy consumption in the U.S. [3]. About 60% of the total renewable energy consumption in the U.S. was in the electric power sector in 2020, and 20% of the total electricity generated was from renewable energy sources [4]. As shown in Figure 1-3, solar energy has emerged as one of the renewable energy sources for the U.S. electricity generation since the late 20th century, and its contribution to the total electricity generation has been increasing to about 11% of renewables and 2.3% of the total U.S. electricity in 2020, which is equivalent to 90.89 billion kilowatthours.

Solar energy includes radiant light and heat from the Sun. As one of the renewable energy sources, solar energy is widely used in many fields. In particular, solar energy can be used even in the mountain-ranged region and developing areas [5]. Solar energy is free and does not harm the environment when it is acquired. However, the shortcomings of solar energy cannot be ignored such as the amount of sunlight due to cloud cover, time of day, and time of year is variable and the photovoltaic process has a low rate of energy conversion [6].

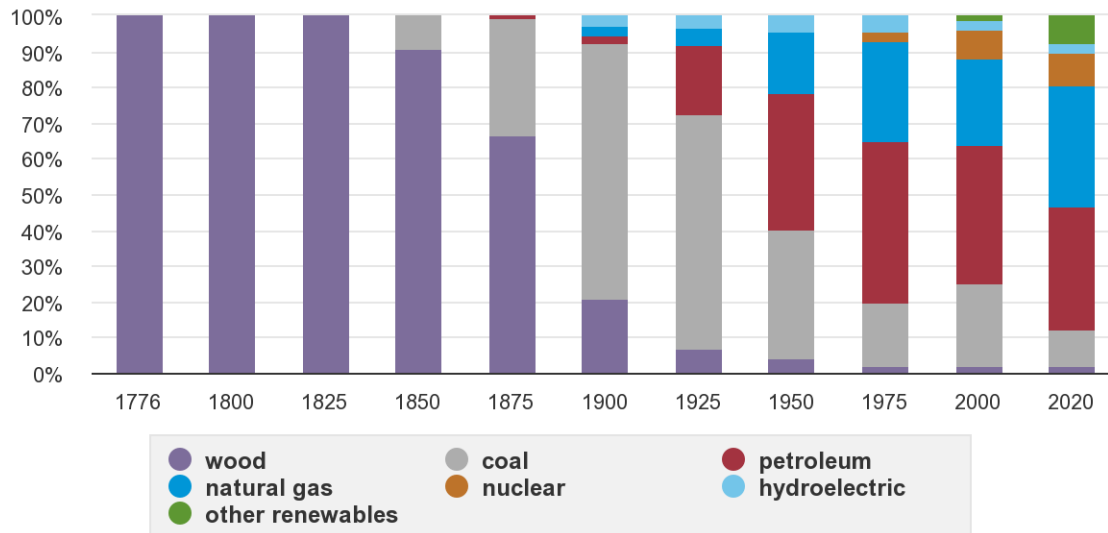


Figure 1-1. Shares of total U.S. energy consumption by major sources in selected years (1776-2020) [3]

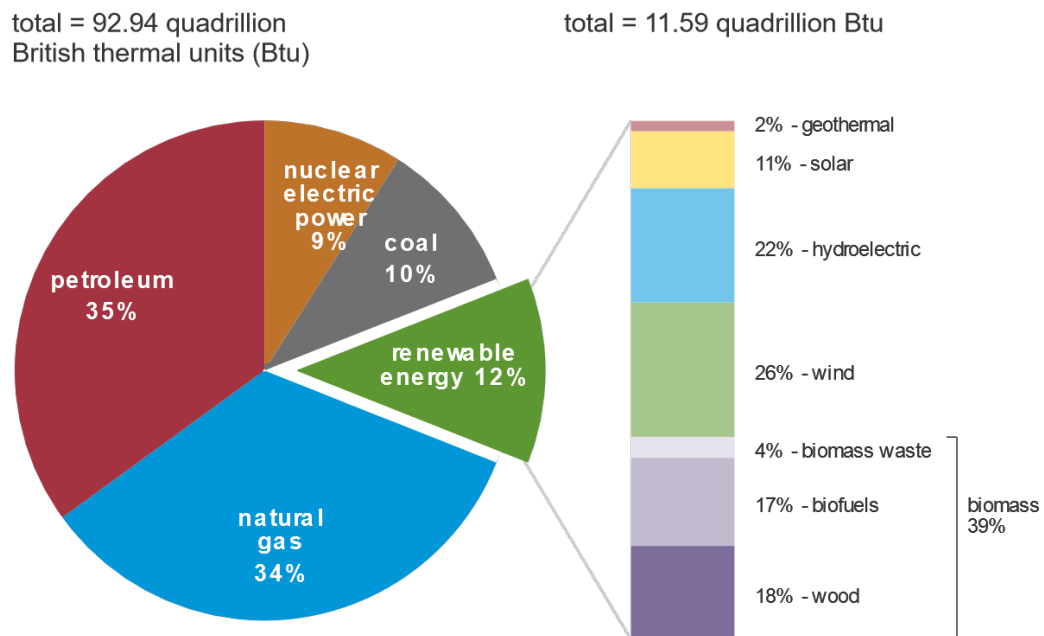


Figure 1-2. U.S. primary energy consumption by energy source in 2020 [3]

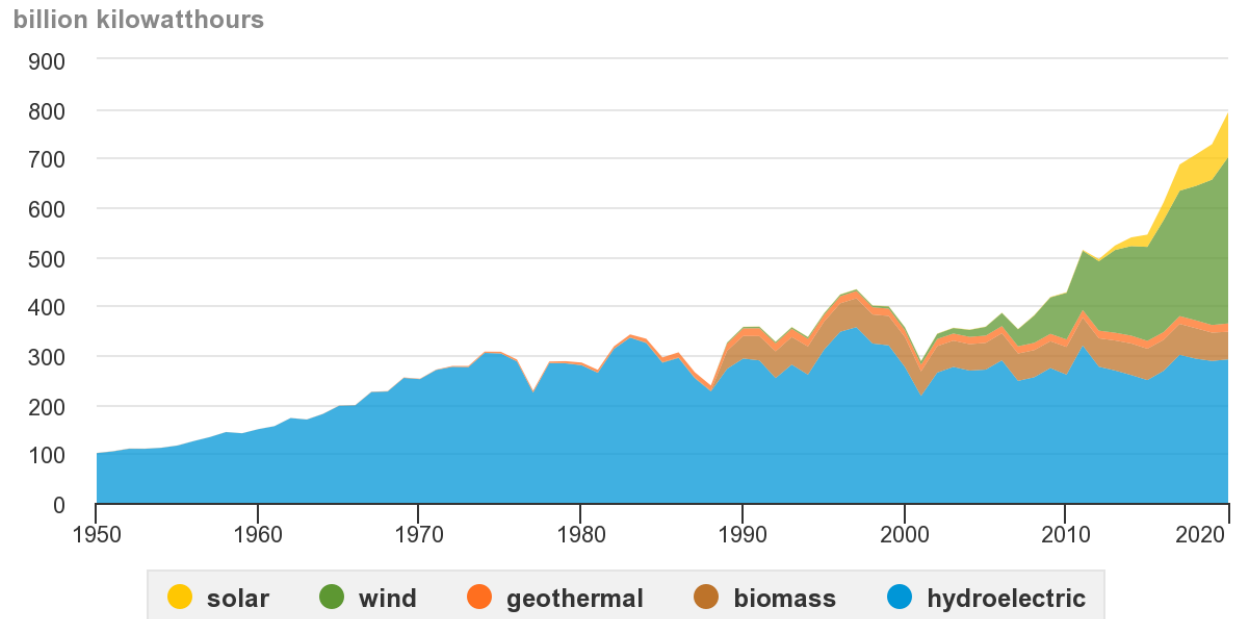


Figure 1-3. U.S. electricity generation from renewable energy sources (1950-2020) [4]

A photovoltaic device, which is also referred to as photovoltaic cell or solar cell, is a nonmechanical device that converts sunlight directly into electricity by the photovoltaic effect [7]. The photovoltaic effect, which was first demonstrated by Edmond Becquerel in 1839, is the generation of voltage and electric current in a material upon exposure to light [8]. A photovoltaic cell is made of semiconductor material such as doped silicon and its electrical characteristics, such as voltage, current, and resistance, vary when exposed to light. Figure 1-4 schematically illustrates the components of a photovoltaic cell and its basic working principle. When sunlight, or photons containing varying amounts of energy that corresponding to the different wavelengths of the solar spectrum, strikes a photovoltaic cell, portions of the sunlight reflect on the surface of the photovoltaic cell, the rest passes through the cell or is absorbed by the semiconductor material. The absorbed photons excite the electrons from their current molecular/atomic orbital and the excited electrons travel through the photovoltaic cell until reaching an electrode. Due to the movement of electrons toward the front surface of the photovoltaic cell, an imbalance of electric charge between the cell's front and back surfaces is created. This imbalance in turn creates a voltage potential. When the cell's front and back surfaces are connected in an electrical circuit to an external load, electricity flows in the circuit [7, 8]. A photovoltaic cell is a building block a photovoltaic system, as shown in Figure 1-5. A single photovoltaic cell can produce a maximum

open-circuit voltage of approximately 0.5 to 0.6 volts [10]. Multiple photovoltaic cells integrated in one plane constitute a solar photovoltaic module. Photovoltaic modules can be connected in groups to form a photovoltaic array, which can be used to charge batteries in the Direct Current (DC) mode, or power devices in the Alternating Current (AC) mode with the help of DC to AC inverters.

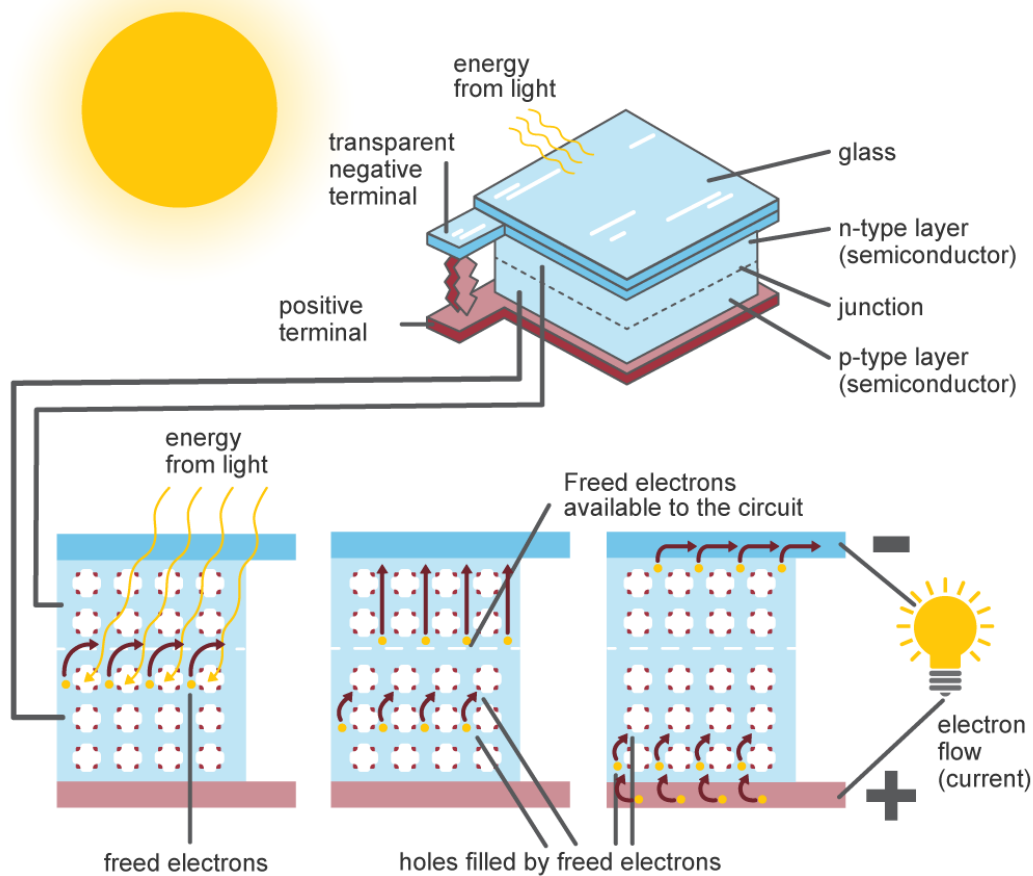


Figure 1-4. Schematic illustration of a photovoltaic cell and its working principle [7].

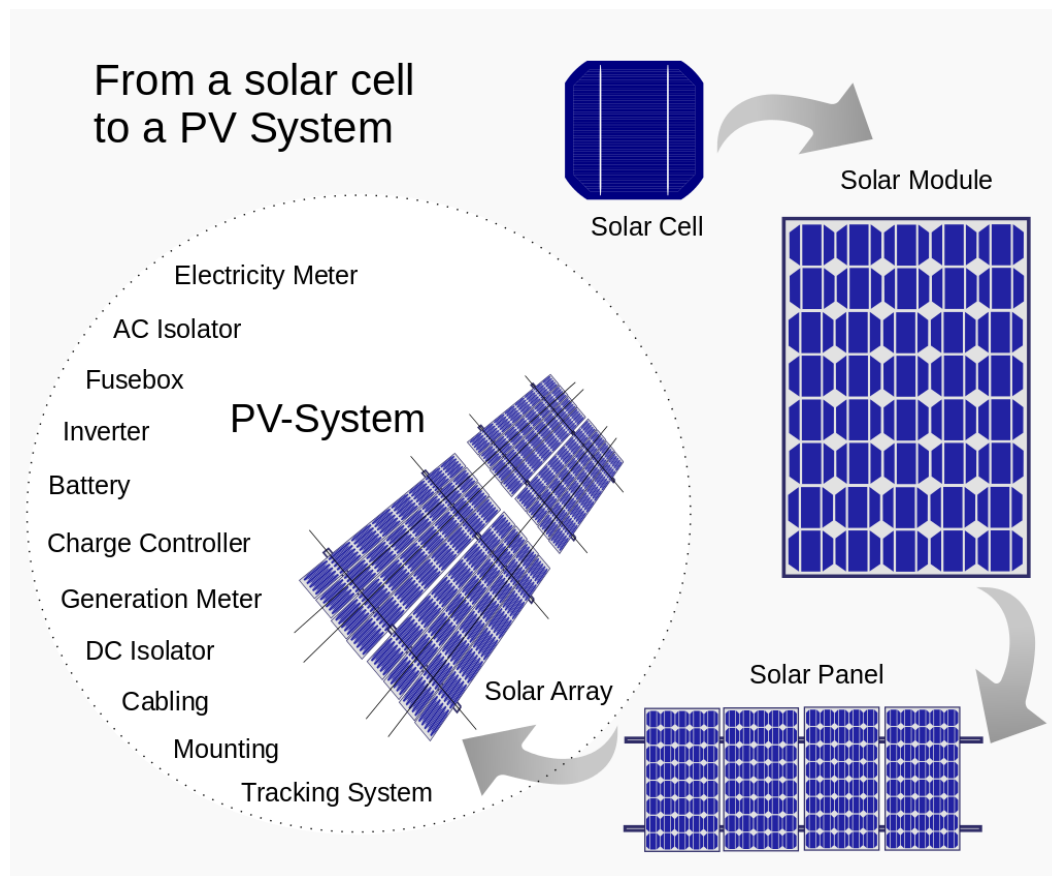


Figure 1-5. Illustration of a photovoltaic system [9]

1.2 Literature review

Photovoltaic systems are one of the promising technologies to collect and convert solar energy to electricity due to the absence of moving mechanical components and relatively low maintenance. The photovoltaic modules can be produced using the standard semiconductor processes with relative minimal facilities [11]. However, due to the high cost of photovoltaic modules, it is essential to optimize the performance of photovoltaic modules.

To analyze the electrical performance of a photovoltaic module, it is common to use the equivalent circuit model of the photovoltaic cell. This model has two main characteristics: current-voltage (I - V) characteristic and power-voltage (P - V) characteristic, both of which characteristics are nonlinear. An important peak exists on the P - V curve, which is called the maximum power point. In order to obtain the maximum possible power from a photovoltaic module, it should be operated at its maximum power point. The output power of photovoltaic modules will be affected by many external factors such as temperature and solar irradiation.

Researchers have utilized circuit topologies to develop the equivalent circuit model to simulate the electrical performance of a photovoltaic module when the environmental conditions such as irradiance and temperature change [12]. Figure 1-6 demonstrates the ideal PV panel model, which is by far the simplest model of the photovoltaic cell. The circuit consists of a current source in parallel to a diode [13, 14]

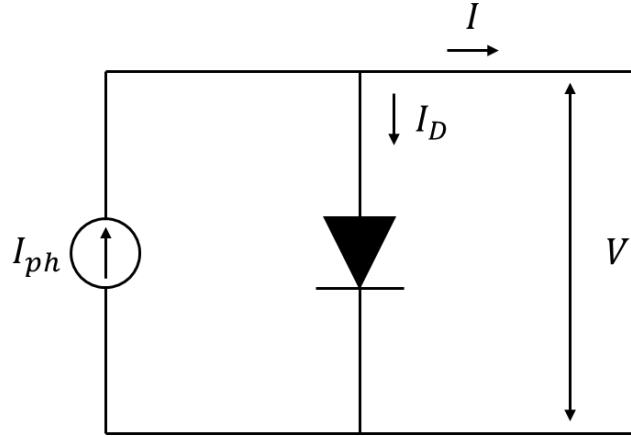


Figure 1-6. An ideal PV panel model [11]

An improved single diode model, as shown in Figure 1-7, adds two resistances. A series resistance, R_s , to represent the resistance in the current path through the semiconductor material, metal grid, contacts, and collecting bus for all of the PV cells in the panel [15-18]. This model is relatively simple when modeling a photovoltaic module in an environment with stable temperature. However, the model becomes less accurate when the surrounding temperature varies to a large extent. It is believed that this deficiency can be eliminated if the open circuit voltage coefficient, K_v , is included in the model [17]. As suggested by many researchers, a parallel (shunt) resistance, R_p , can be added to the circuit to represent the leakage current of the p-n junction for all of the PV cells in the panel [19-22]. The corresponding circuit is shown in Figure 1-8. By adding R_p in the circuit, the number of model parameters increases to five, thereby significantly enhancing the accuracy of the modeling.

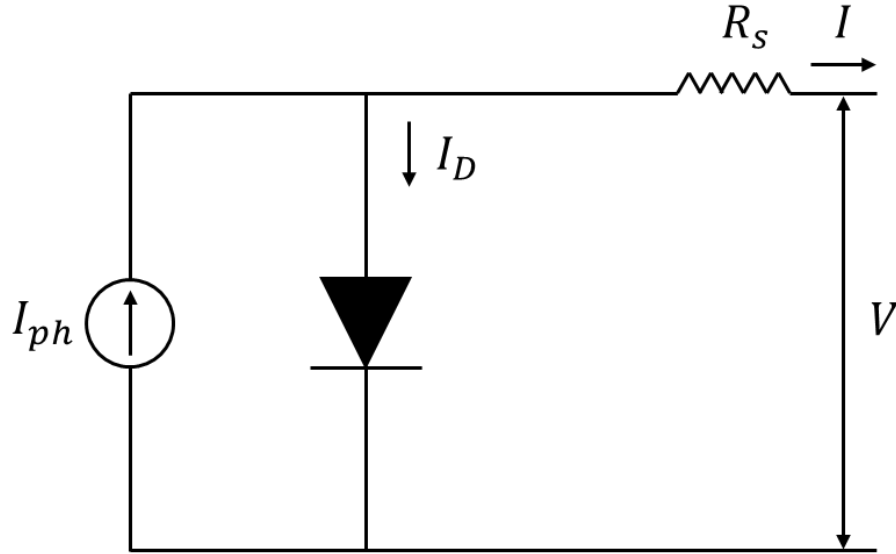


Figure 1-7. Improved single diode equivalent circuit

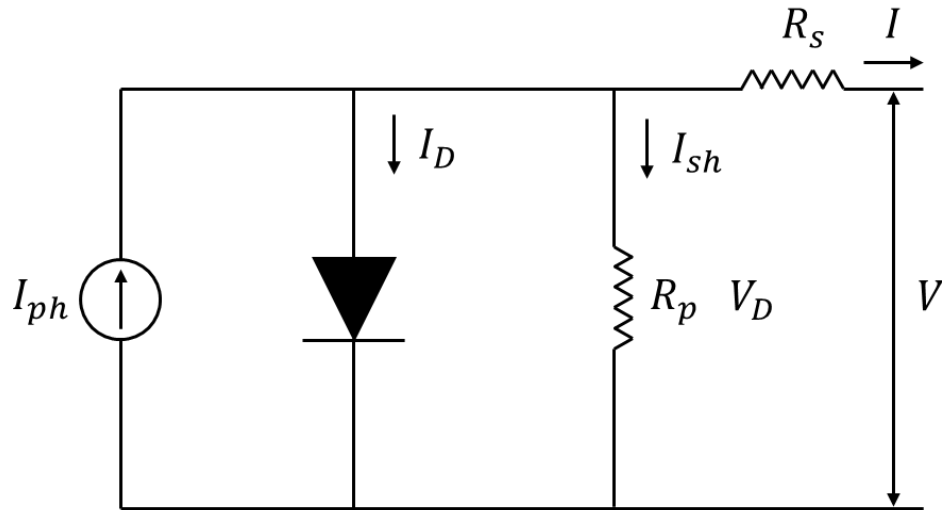


Figure 1-8. Extension of the improved single diode equivalent circuit [11]

Although the improved single diode model is accurate for most of the operating conditions, it neglects the recombination loss in the depletion region. Such assumption becomes inadequate when the recombination loss is substantial. Therefore, a second diode is added to the circuit when recombination in the junction dominates at lower voltages and to improve the inaccuracies of the single diode model near the maximum power point [23]. Figure 1-9 shows the equivalent circuit of a double circuit model. As mentioned previously, the addition of model parameters can greatly

improve the modeling accuracy, but it also poses challenges when numerically solving the model. The primary challenge is to accurately estimate the value, or the range, of each model parameter without compromising the overall accuracy and with a reasonable computational effort [12].

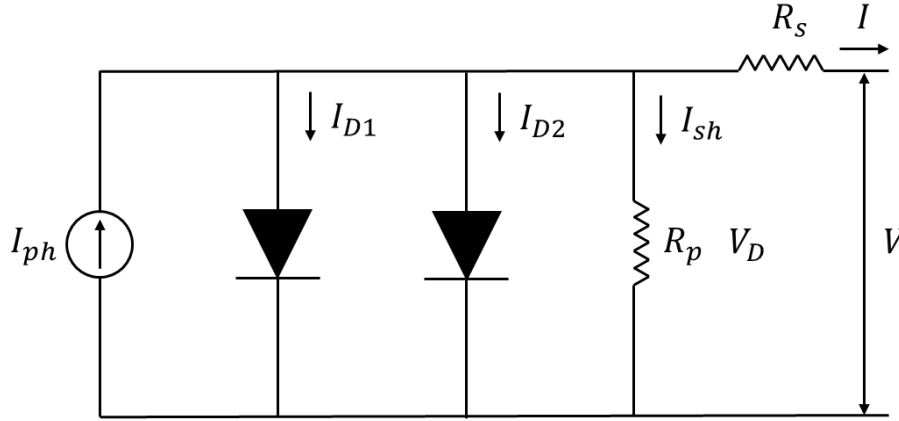


Figure 1-9. Double diode equivalent circuit

To accurately and efficiently evaluate the model parameters, previous researchers have proposed various numerical methods. For instance, Xiao et al. [16] and Matagne et al. [24] developed an iterative method to estimate the value of the series resistance, R_s , and the diode ideality, n , in the improved single diode model, which includes four model parameters, namely R_s , n , I_{sc} (short circuit current), and I_o (saturation current). The values of these four model parameters are further refined by the interpolating technique [18]. If the parallel resistance, R_p , is considered, other numerical algorithms such as resistive-companion method [19], non-linear least square optimization algorithm [20], and several other methods [21, 22] can be adopted. More recently, researchers have utilized artificial intelligence (AI) to estimate the model parameters. For example, Elshatter et al. have adopted fuzzy logic to model the photovoltaic system [25]. Others have applied artificial neural networks to model the photovoltaic cells and have produced reasonably accurate results [26-29]. However, the AI techniques require significant amount of computational power compared to the iterative method. The computational time drastically increases as the number of model parameters increase. Another disadvantage of the AI techniques is that a separate set of data is required for training. The accuracy of the training also depends on the size of the training data. For simulations with limited number of data sets, the previous iterative method is recommended.

Similarly, various computational methods have been proposed for the double diode model. For instance, Gow and Manning have applied curve fitting technique which proposed by Levenberg and optimized by Marquardt to construct the I - V curves [30, 31]. Chowdhury et al. developed an equivalent Thevenin circuit to estimate the model parameters [32]. Whereas Hovinen formulated the model parameters as a function of series resistance [33]. One of the disadvantages of these methods is that new coefficients were added into the governing equations, which would require more computational efforts to solve.

By acknowledging the deficiencies in the previous methods, other researchers developed physical based solutions. Several physical characteristics such as the electron diffusion coefficient, minority carrier's lifetime, intrinsic carrier density, and other semiconductor parameters [12] have been considered when describing the double diode model. Methods using this approach include the irradiance decrease open circuit measured method [34], diffusion-current dominant area (DCA) and a recombination-current dominant area (RCA) [35], modified double diode equivalent circuit model [36], and the modified three-diode model for multicrystalline silicon (Mc-Si) solar cells [37]. The physical-based approach is useful when the physical behaviors of the photovoltaic cell are required. The main challenge is to evaluate the semiconductor parameters, which are not always available from the manufacturers' datasheet [12]. In addition, the aforementioned physical-based methods assume that the diode ideality factors $n_1 = 1$ and $n_2 = 2$. Although this assumption has been adopted by most of the researchers, some researchers have assumed that $n_1 = 1$ and $n_2 \geq 1.2$ [38-42]. Gupta et al. assumed that $n_1 = 1$, $n_2 = 1$, and $R_{sh} = \infty$ [43]. Elbaset et al. have taken a different approach by considering the sum of n_1 and n_2 for different solar cells. They assumed $n_1 + n_2 = 3$ for polycrystalline solar cells and $n_1 + n_2 = 4$ for amorphous solar cells [44].

1.3 Objectives

As discussed in the previous section, the single diode model is relatively simple and requires an insignificant amount of computational time, but it would fail if the recombination loss were substantial. The double diode model was proposed to represent the recombination loss and improve accuracy, but at the cost of adding more parameters to the model. The primary challenge to applying the double diode model is obtaining the optimum value for each model parameter while maintaining a reasonable computational effort.

Therefore, the current study is intended to develop an estimation method for the parameters of the double diode model. The approach will be to investigate the effect of each parameter in the double diode model. Propose a method to obtain an initial estimate for each of the seven model parameters from data provided by the manufacturer. Using these initial estimated parameters as inputs, apply the Newton-Raphson method to improve parameter estimates and prediction accuracy. Model the performance of two PV modules from different manufacturers using the initial parameter estimates and the Newton-Raphson updated parameters. Compared modeled I - V and P - V curves to the manufacturers' data.

2. METHODOLOGY

In order to plot the current-voltage (I - V) characteristic curve and power-voltage (P - V) characteristic curve for a photovoltaic panel, an equivalent circuit model is developed. During this development two equivalent circuit models are developed in this study (i.e., one diode model and double diode model), which can be used to evaluate the performance of PV cells and the effect of each component. The simulation is conducted in MATLAB 2020b and Simulink. The inputs of the model are temperature and irradiance. When studying the influence of the model parameters such as R_s , R_p , n and I_o on the outputs, the standard test environment is assumed: temperature of cell is 25 °C and the solar irradiance is 1000 W/m².

2.1 One diode model

2.1.1 Mathematic model

A photovoltaic (PV) panel is composed of photovoltaic cells connected in series. Each photovoltaic cell consists of a semiconductor device with a p-n junction [11]. For this reason, the most basic model for a photovoltaic panel uses a simple diode model, as shown in Figure 2-1.

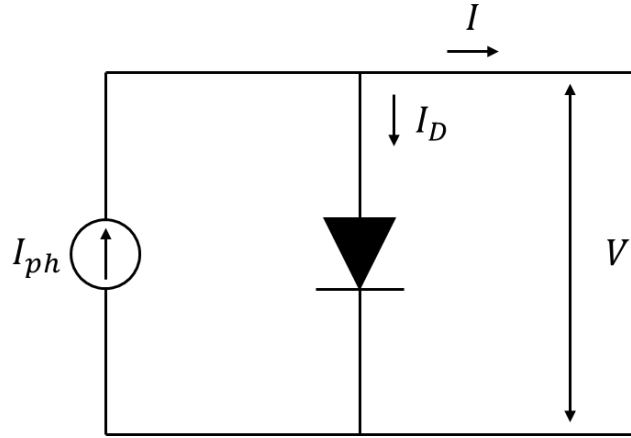


Figure 2-1. An ideal PV panel model [11]

Using Kirchhoff's current law, I , of the PV panel is represented by the following equation:

$$I = I_{ph} - I_o \left[\exp \left(\frac{V_D}{nV_T} \right) - 1 \right] \quad (2-1)$$

Where I_{ph} is the photo-generated current, I_o is the saturation current, V_D is the voltage across the p-n junction (which is equal to V , the output voltage of the PV panel, for this model), n is the diode ideality factor (which varies between 1 and 2 depending upon the fabrication process and semiconductor material and in many cases is assumed to be 1), and V_T is the thermal voltage of the PV panel. V_T is determined using [11]:

$$V_T = \frac{N_s k T}{q} \quad (2-2)$$

Where N_s is the number of photovoltaic cells connected in series to form the PV panel, k is Boltzmann's constant (1.281×10^{-23} J/K), T is the temperature in degrees Kelvin (K), and q is the electron charge (1.602×10^{-19} C).

Comparing the I - V curves from the manufacturer of a photovoltaic panel in widespread use from Trina Solar to those generated using Eq. (2-1) (see Figure 2-2), it is apparent that Eq. (2-1) cannot represent the characteristics of the PV panel accurately in a low irradiance environment.

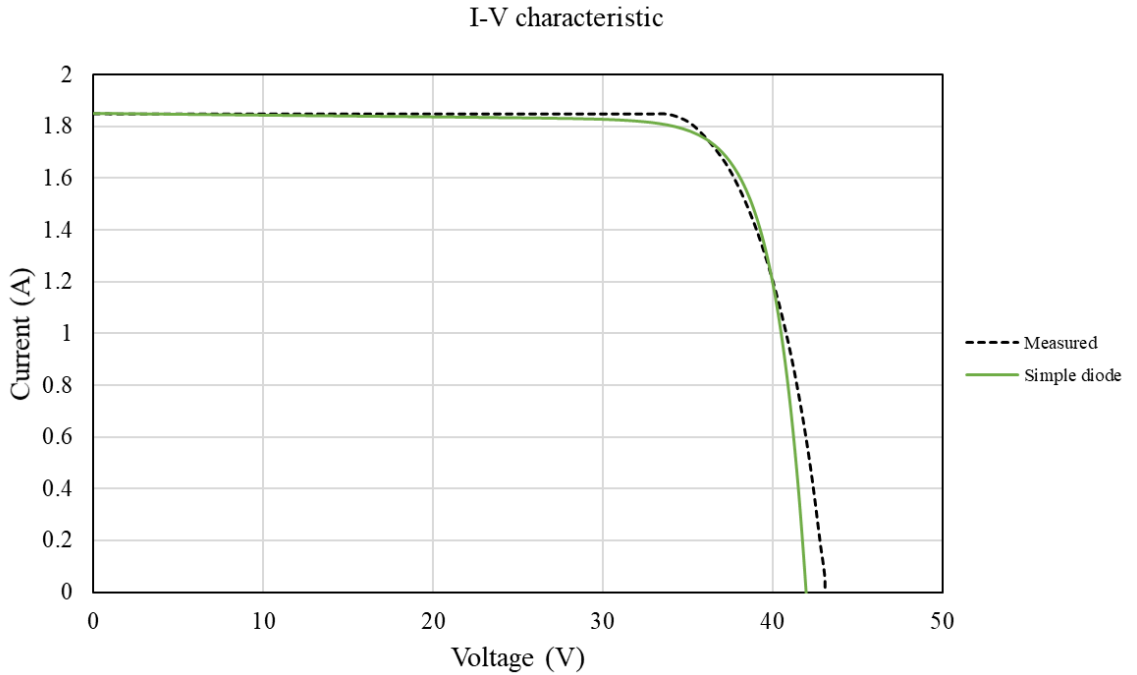


Figure 2-2. Comparison of manufacture's I - V curve with the simple diode model under the irradiance of 200W/m^2

The simplicity of the ideal PV model does enable us to understand the effects of I_o , the saturation current, and n , the diode ideality factor on the I - V curves. Figure 2-3 demonstrates the effect of different values of I_o while keeping n fixed at 1. Figure 2-4 demonstrates the effect of different values of n while keeping I_o keeping fixed at 1.3×10^{-10} .

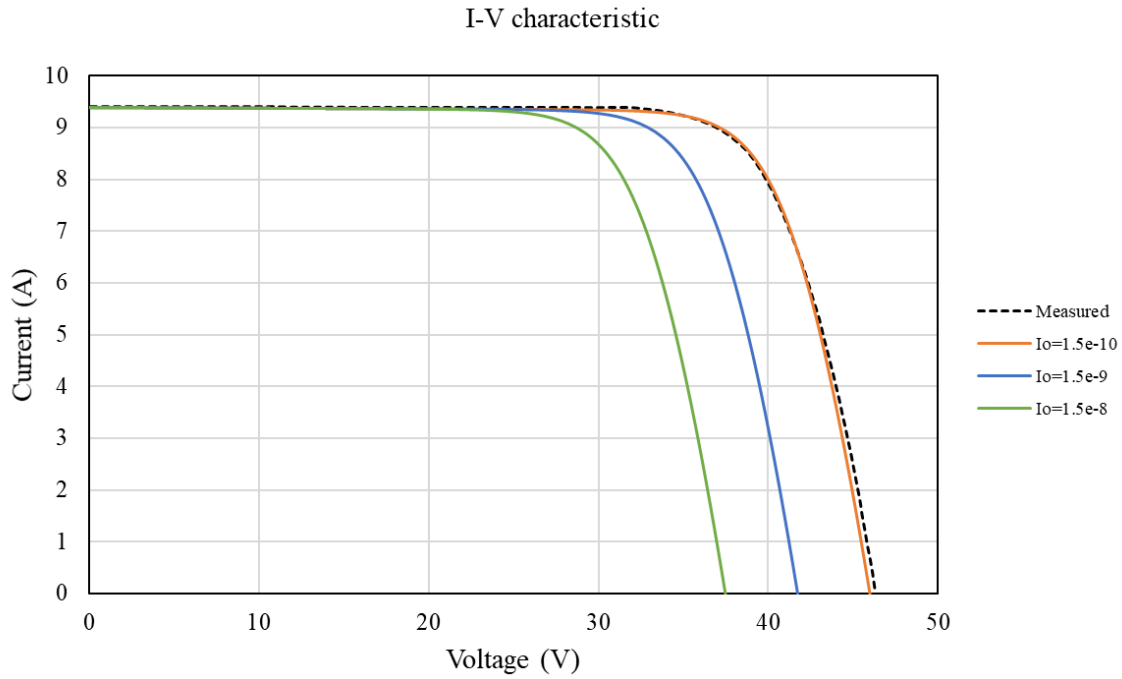


Figure 2-3. Effect of I_o on the simple PV panel I - V Model for $n = 1$

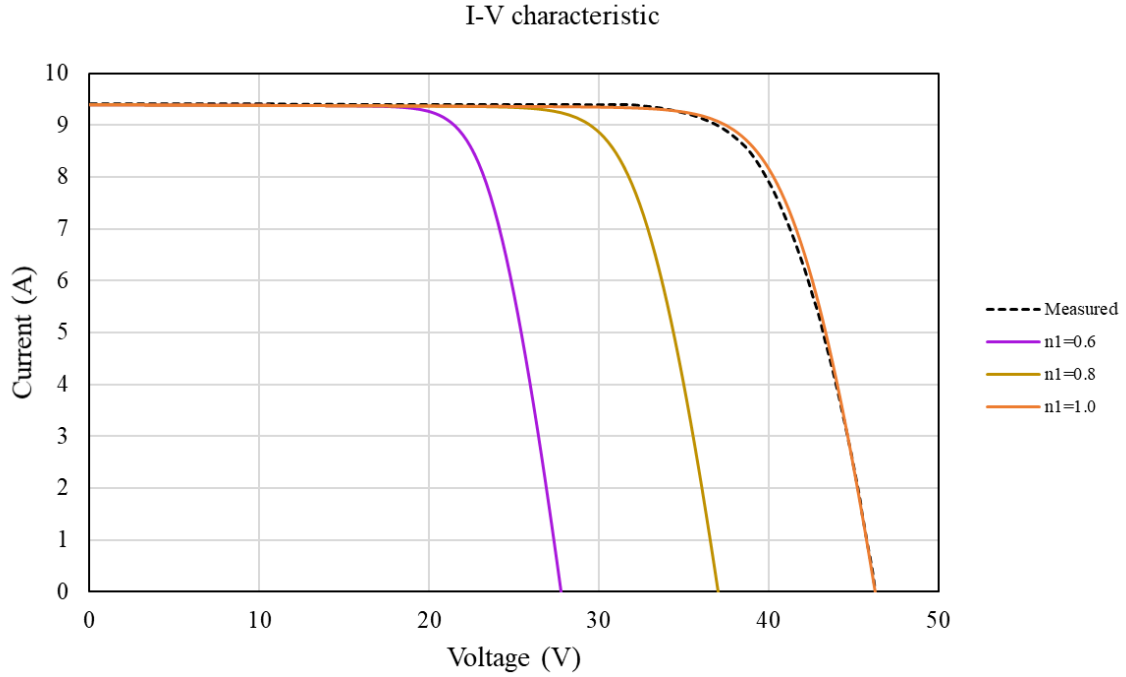


Figure 2-4. Effect of n on the simple PV panel I - V Model for $I_0 = 1.3 \times 10^{-10}$

From Figure 2-3 it can be seen that the larger I_0 , the sooner and more pronounced the dip in the I - V curve. From Figure 2-4 it can be seen that the smaller n , the sooner and more pronounced the dip in the I - V curve. This information will be useful when determining parameters for the more complicated models.

A more accurate single diode model, shown in Figure 2-5, adds two resistances. A series resistance, R_s , to represent the resistance in the current path through the semiconductor material, metal grid, contacts, and collecting bus for all of the PV cells in the panel [15]. A parallel (shunt) resistance, R_p , to represent the leakage current of the p-n junction for all of the PV cells in the panel.

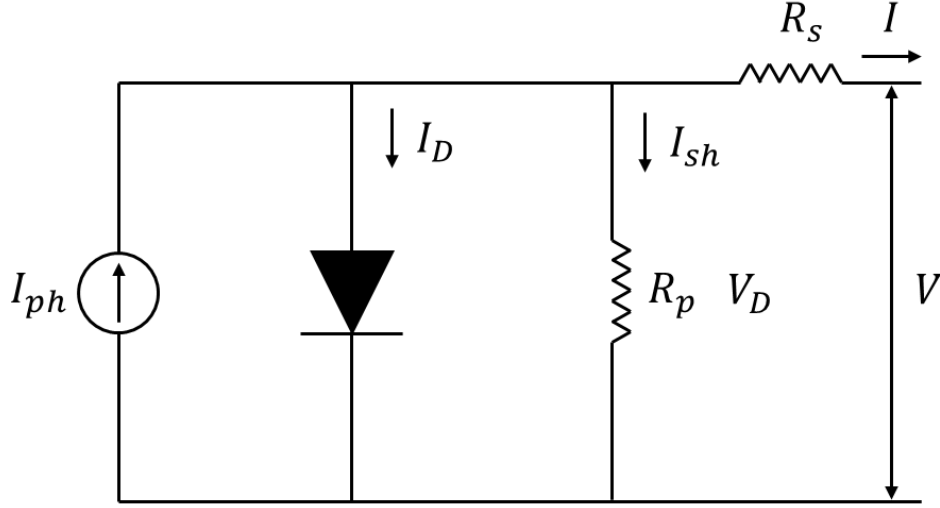


Figure 2-5. Single diode equivalent circuit [11]

Using Kirchhoff's current law (KCL), Kirchhoff's voltage law (KVL), and Ohms law, the following equations can be obtained:

$$I = I_{ph} - I_D - I_{sh} \quad (2-3)$$

$$V_D = V + IR_s \quad (2-4)$$

$$V_D = I_{sh}R_p \quad (2-5)$$

Equating Eq. (2-4) and Eq. (2-5) and solving for I_{sh} , yields:

$$I_{sh} = \frac{V_D}{R_p} = \frac{V + IR_s}{R_p} \quad (2-6)$$

I_D shown in Eq. (2-3) is the same as Eq. (2-1) [45]:

$$I_D = I_o \left(\exp \frac{V_D}{nV_T} - 1 \right) \quad (2-7)$$

Substituting Eq. (2-2) and Eq. (2-4) into Eq. (2-7) and substituting Eq. (2-6) and Eq. (2-7) into Eq. (2-3), the following five-parameter single diode model can be obtained:

$$I = I_{ph} - I_D - I_{sh} = I_{ph} - I_o \left\{ \exp \left[\frac{q(V + IR_s)}{nN_s kT} \right] - 1 \right\} - \frac{V + IR_s}{R_p} \quad (2-8)$$

2.1.2 Characteristics of I - V and P - V curves of the single diode model

Figure 2-6 compares the I - V characteristic predicted by Eq. (2-1) and Eq. (2-8) and Figure 2-7 compares the output power versus voltage, P - V , characteristic predicted by Eq. (2-1) and Eq.

(2-8). From Figure 2-6 and Figure 2-7 it is easily seen that the models produce different results near the maximum power output of the PV panel, which is where one would like to operate a PV panel.

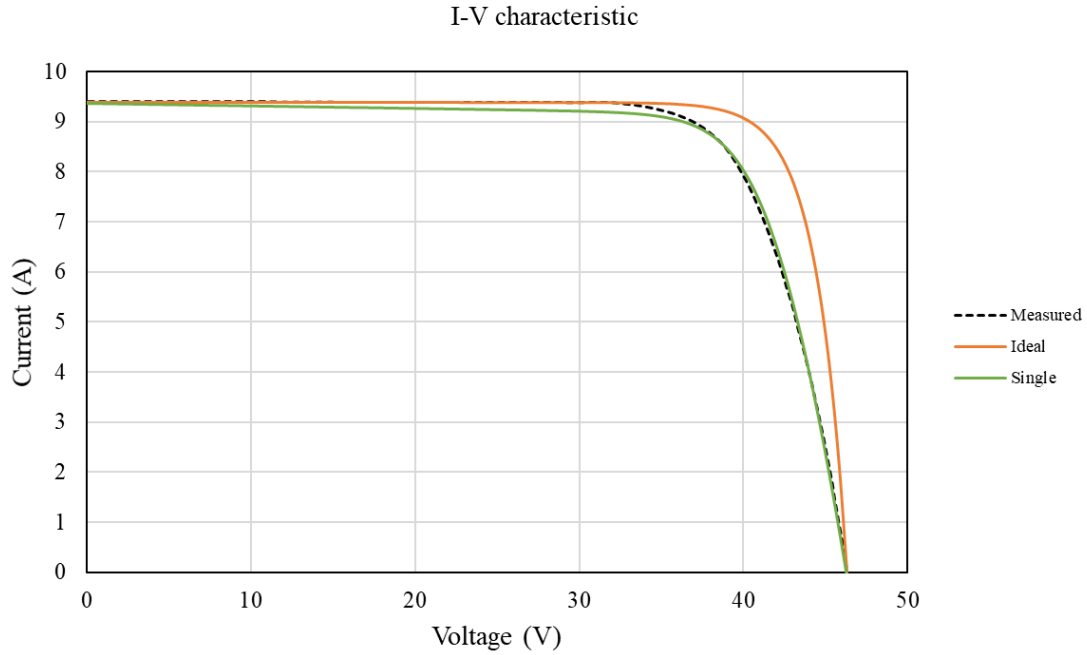


Figure 2-6. *I-V* characteristic of the single diode model and ideal model

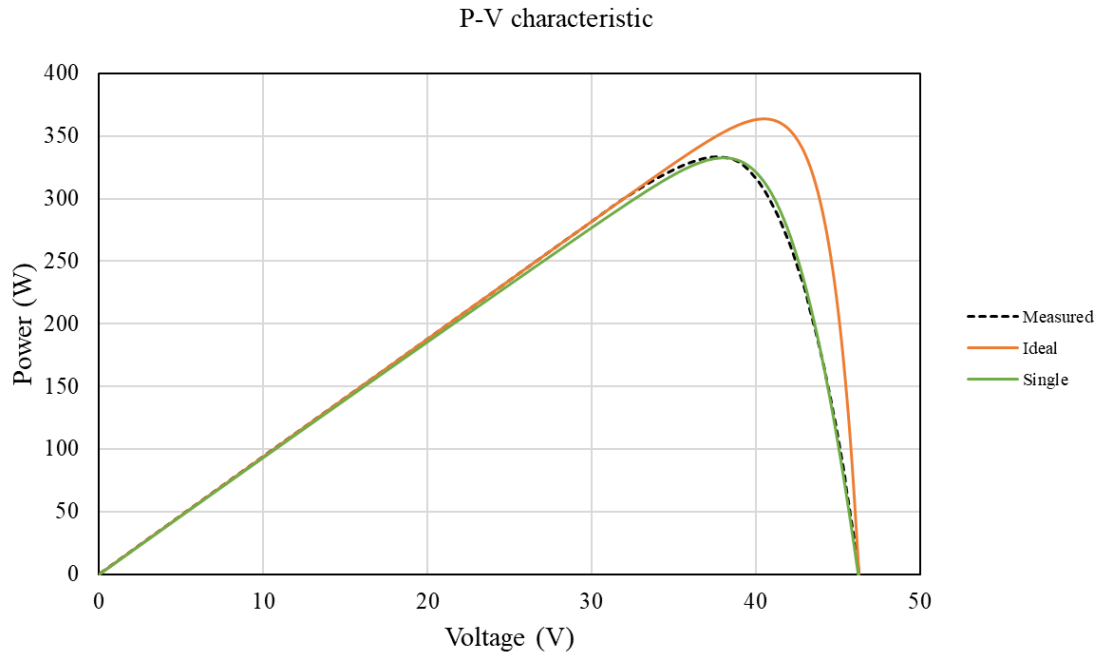


Figure 2-7. *P-V* characteristic of the single-diode model and ideal model

Figure 2-8 and Figure 2-9 illustrate the effect of R_p on the I - V and P - V characteristics. All the other model inputs are kept constant to isolate the effect of R_p . From Figure 2-8, it is apparent that R_p determines the slope of the I - V curve before the exponential term in (2-8), due to the diode, dominates the response. Since the current, I , in Eq. (2-8), is affected by the current, I , in the exponent, the size of R_p also affects the exponential portion of the response. From Figure 2-8, it is also apparent that as V increases and I decreases the effect of R_p becomes negligible. Note that while R_p determines the slope of the I - V curve at $V = 0$, it does not determine the size of the current at $V = 0$ (I_{SH}) and does not affect the size of the voltage at $I = 0$ (V_{OC}). Furthermore, the current and the output power are more sensitive to the change of R_p when the value of R_p is smaller than 100. When R_p is larger than 300, the outputs are insensitive to the change of R_p .

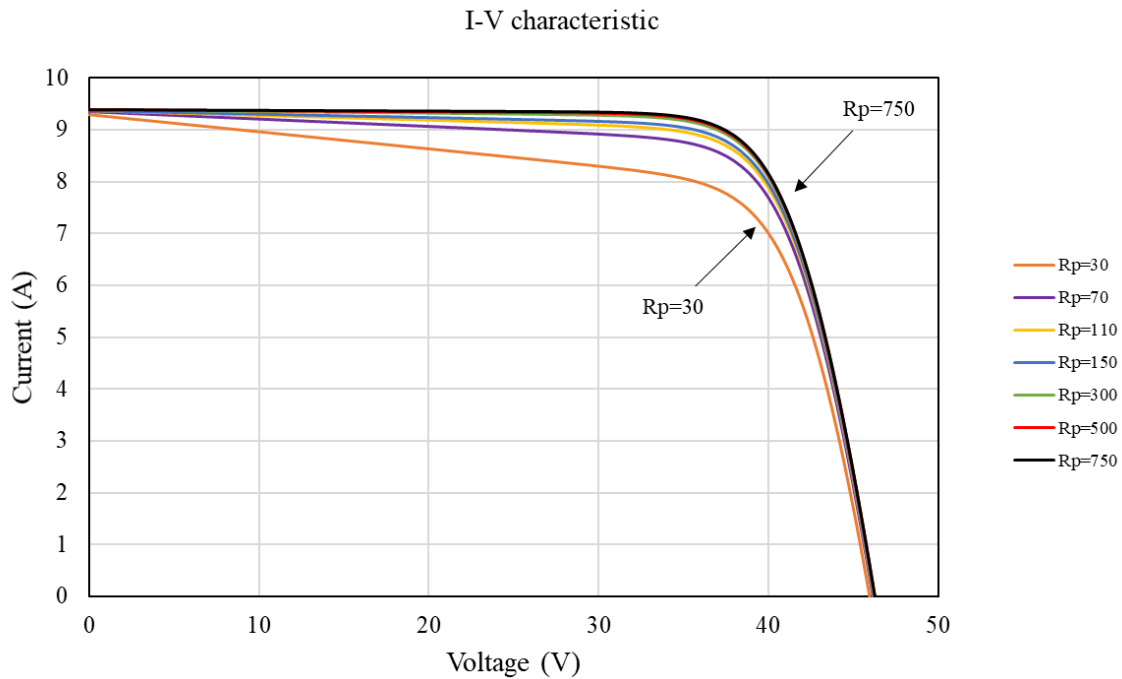


Figure 2-8. I - V curve in response to the change of R_p

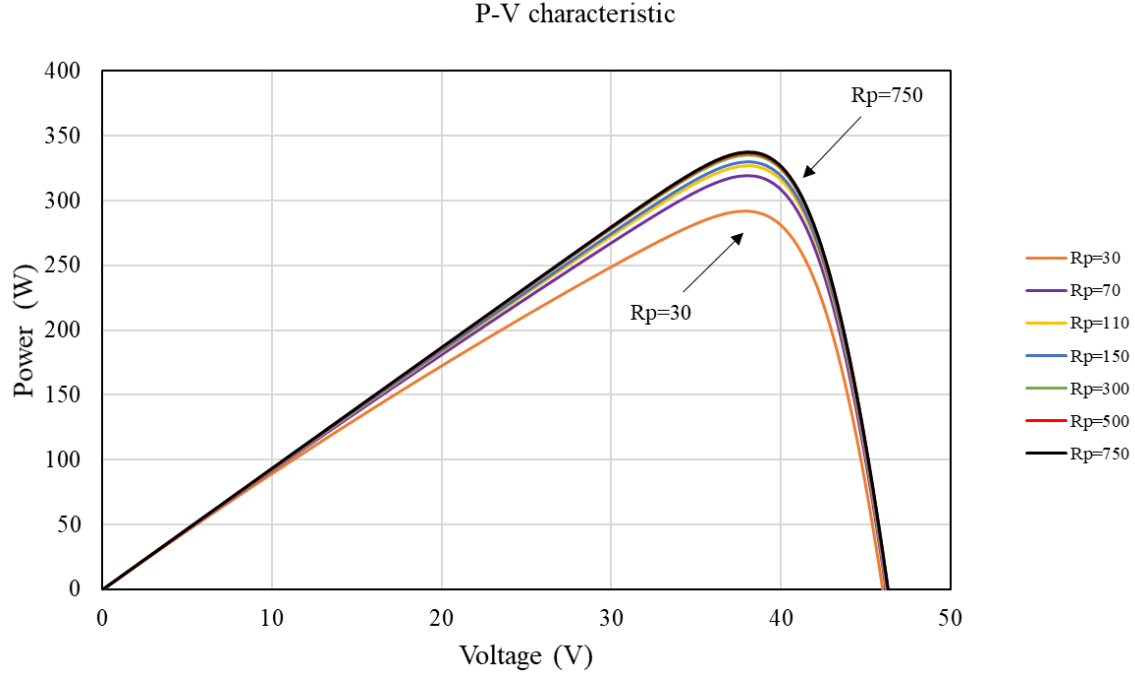


Figure 2-9. P - V curve in response to the change of R_p

Figure 2-10 and Figure 2-11 demonstrate the effect of R_s on the I - V and P - V characteristics. All the other model inputs are kept constant to isolate the effect of R_s . From Figure 2-10, it is apparent that R_s affects the slope of the I - V curve at $I = 0$ (V_{OC}) and since it also appears in the exponential term in Eq. (2-8), due to the diode, R_s also affects the exponential portion of the response. Note that while R_s affects the slope of the I - V curve at $I = 0$, it does not determine the size of the voltage, V_{OC} , at $I = 0$ and does not affect the size of the current, I_{sc} , at $V = 0$. Furthermore, the current in the I - V curve is somewhat uniformly sensitive to the change of R_s .

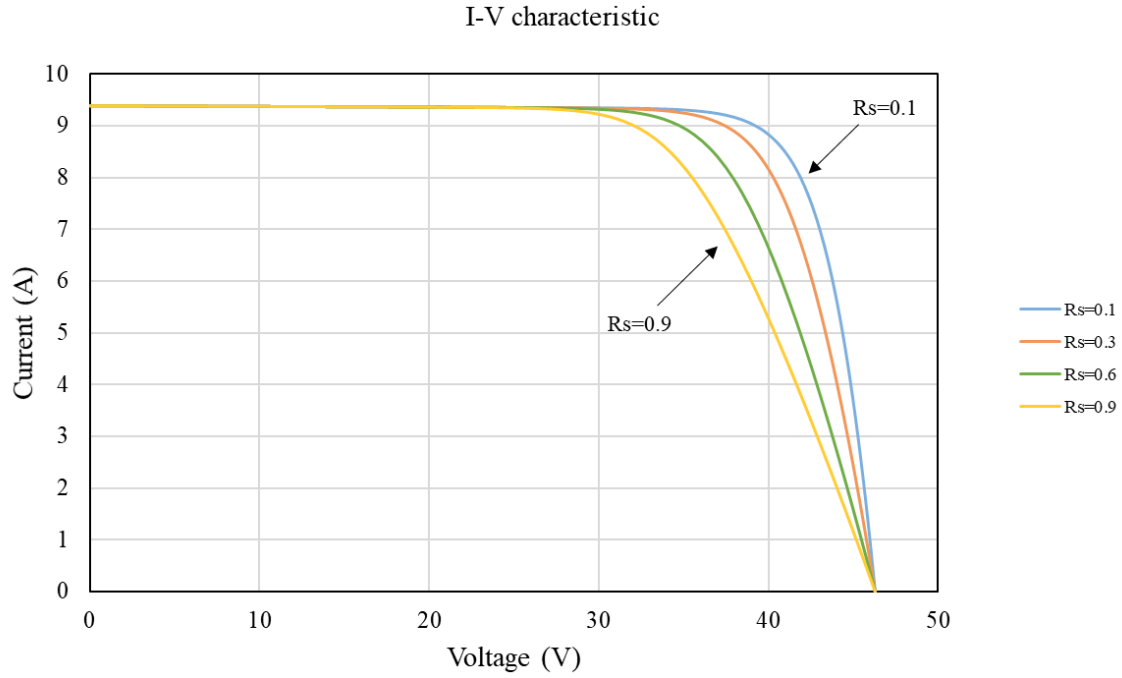


Figure 2-10. I - V curve in response to the change of R_s when $R_p = 750$

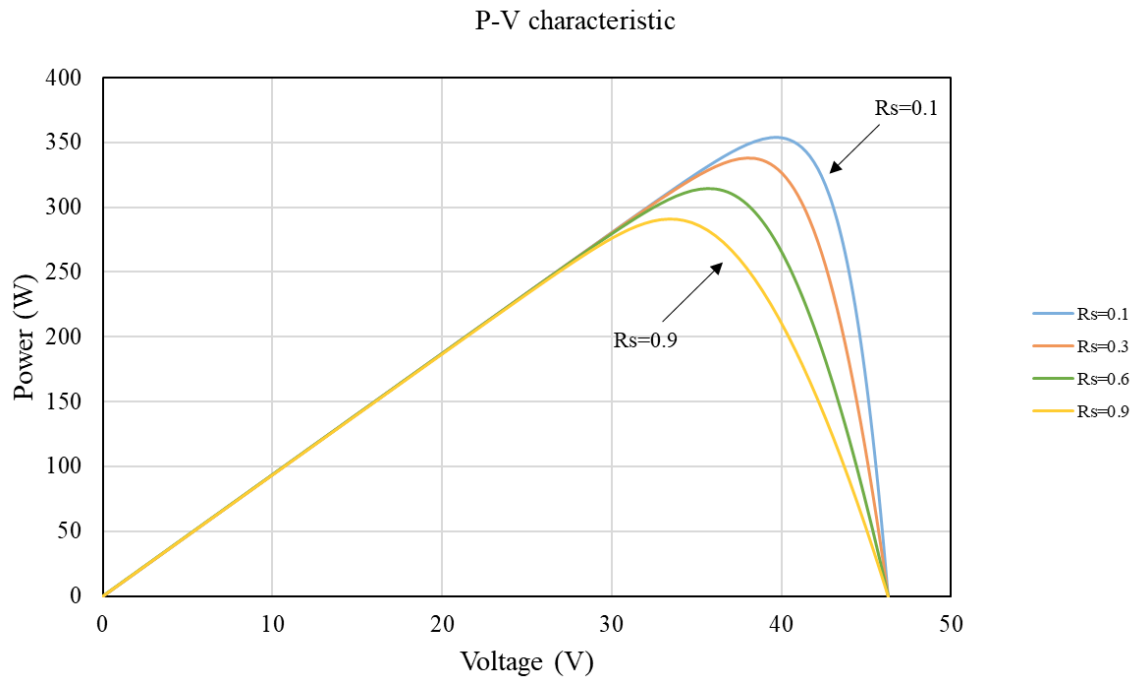


Figure 2-11. P - V curve in response to the change of R_s when $R_p = 750$

2.2 Double diode model

2.2.1 Mathematic model

The double diode equivalent circuit is shown in Figure 2-12. An additional diode is added to the circuit compared to the single diode model shown in Figure 2-5. The second diode is used when recombination in the junction dominates at lower voltages and to improve the inaccuracies of the single diode model near the maximum power point [23].

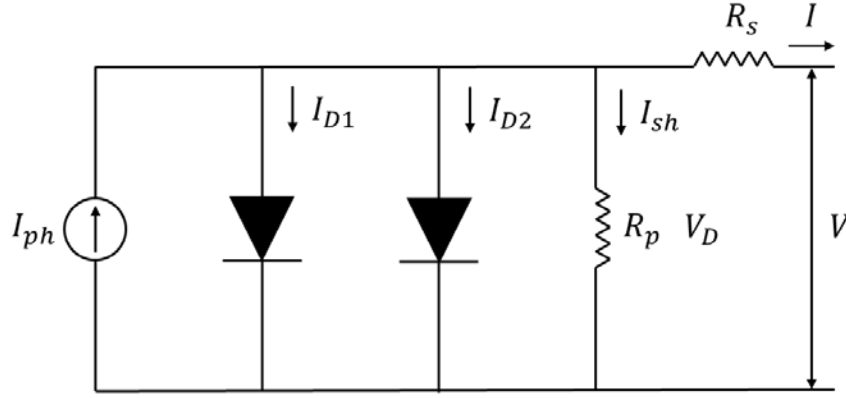


Figure 2-12. Double diode equivalent circuit

Using KCL, KVL, and Ohm's law, the following equations can be obtained:

$$I = I_{ph} - I_{D1} - I_{D2} - I_{sh} \quad (2-9)$$

$$V_D = V + IR_s \quad (2-10)$$

$$V_D = I_{sh}R_p \quad (2-11)$$

Following the same process used for the single diode model in Eq. (2-8) with the exception that each diode has its own saturation current, I_{oi} , and diode ideality factor, n_i ,

$$I_{Di} = I_{oi} \left\{ \exp \left[\frac{q(V + IR_s)}{n_i N_s k T} \right] - 1 \right\} \quad (2-12)$$

The following seven-parameter, double diode model is obtained:

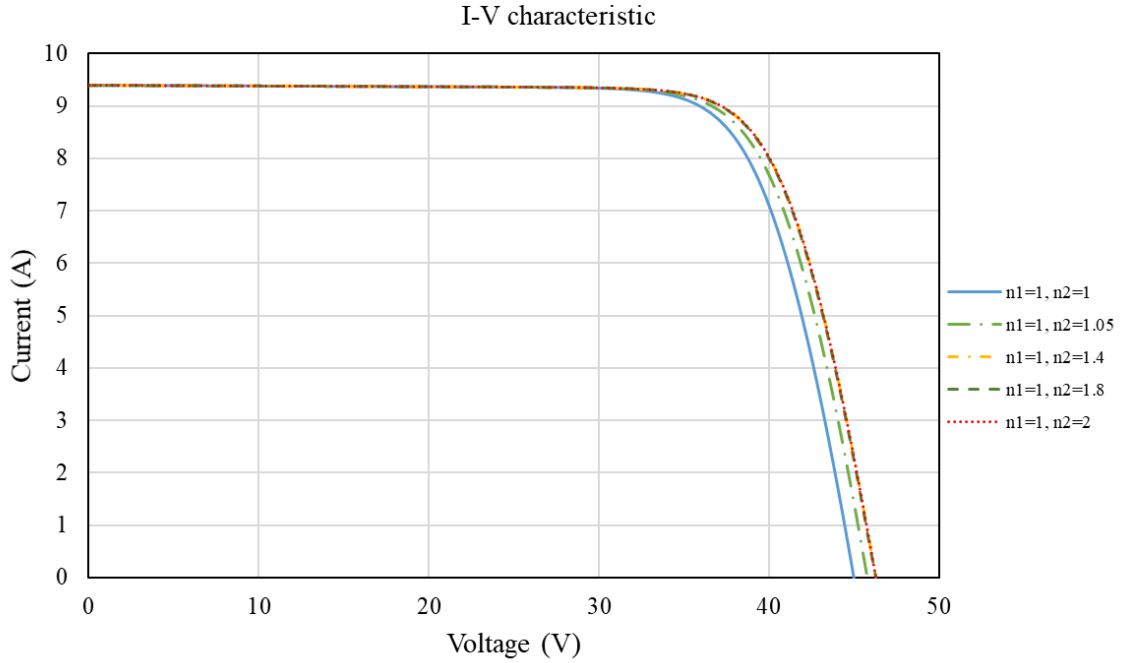
$$\begin{aligned} I &= I_{ph} - I_{D1} - I_{D2} - I_{sh} \\ &= I_{ph} - I_{o1} \left\{ \exp \left[\frac{q(V + IR_s)}{n_1 N_s k T} \right] - 1 \right\} - I_{o2} \left\{ \exp \left[\frac{q(V + IR_s)}{n_2 N_s k T} \right] - 1 \right\} \\ &\quad - \frac{V + IR_s}{R_p} \end{aligned} \quad (2-13)$$

As shown in Eq. (2-13), the current, I , is affected by I_{ph} , R_s , R_p , I_{o1} , I_{o2} , n_1 , and n_2 . The panel voltage, V , is the dependent variable. The number of cells in the panel, N_s , is provided by the manufacturer. The operating temperature, T , is known, and k and q are known constants. The effect of R_s and R_p have been discussed in the previous section.

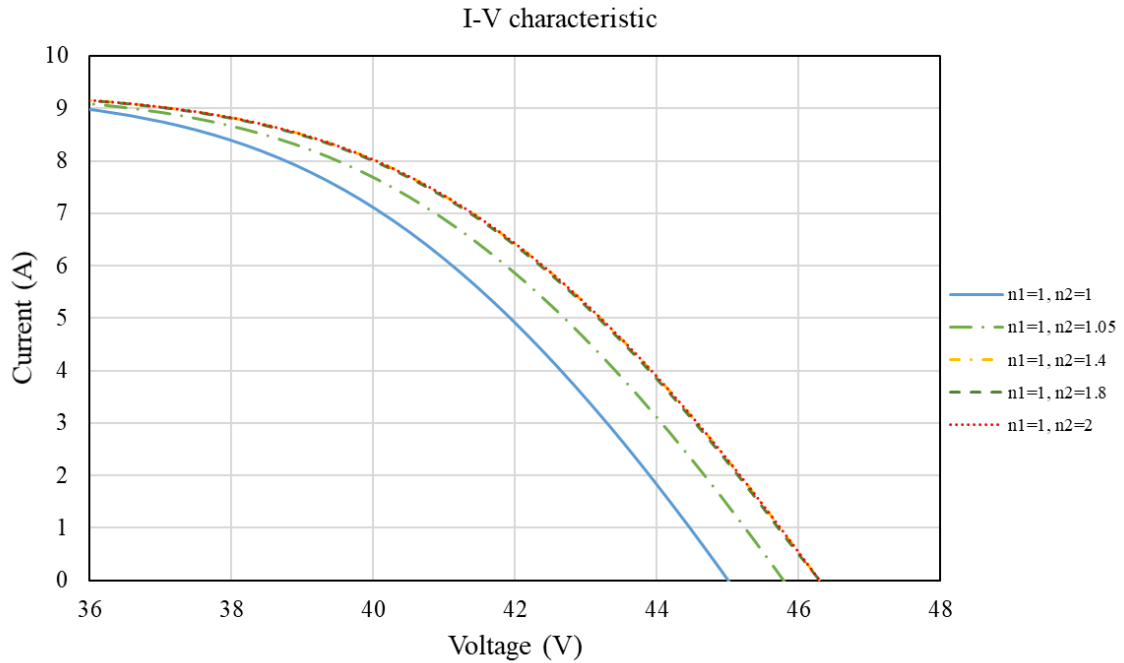
2.2.2 Sensitivity of n_2

n_1 and n_2 shown in Eq. (2-13) are the diode ideality factors. The values of n_1 and n_2 vary in the literature. Most of the previous works have assumed the value of n_1 to be unity and the value of n_2 to be 2 [46-53]. Some of the researchers assumed that $n_1 = 1$ and $n_2 \geq 1.2$, while $I_{o1} = I_{o2}$ [38-42]. Gupta et al. assumed that $n_1 = 1$, $n_2 = 1$, and $R_{sh} = \infty$ [43]. Elbaset et al. have taken a different approach by considering the sum of n_1 and n_2 for different solar cells. They assumed $n_1 + n_2 = 3$ for polycrystalline solar cells and $n_1 + n_2 = 4$ for amorphous solar cells [44]. Since monocrystalline solar cells are being modelled in the current study, the value of n_1 is assumed to be unity as suggested by most of the previous works, and the value of n_2 varies from 1 to 2.

Figure 2-13 (a) and (b) show the variation of the I - V characteristics in response to the change of n_2 while keeping $I_{o1} = I_{o2} = 1.3 \times 10^{-10}$. The current is insensitive to the value of n_2 until the voltage is larger than 30 V, beyond which the current starts to decrease at larger voltages as the value of n_2 increases from 1 to 2. The difference in the current is evident when the value of n_2 is smaller than 1.2, as shown in Figure 2-13 (a). When $n_2 > 1.2$, the change of the current at different values of n_2 is barely noticeable, as shown in Figure 2-13 (b). Hence, the effect of n_2 is to slightly increase the current near the maximum power point as n_2 increases from 1 to 1.2. After that, further increase of n_2 has negligible effect on the current. Increasing the value of n_2 also changes the value of the voltage, V_{oc} , ($I = 0$), but does not affect the value of the current, I_{sc} , ($V = 0$).



(a)



(b)

Figure 2-13. I - V curve in response to the change of n_2 : (a) the full range, and (b) enlarged view

Figure 2-14 (a) and (b) show the variation of the P - V characteristics in response to the change of n_2 . Similar to the I - V characteristics, the output power is only sensitivity to the value of n_2 when the voltage is larger than 30 V. The size and location of the output power also increases as n_2

increases from 1 to 1.2. Once the value of n_2 is larger than 1.2, the output power is insensitive to the value of n_2 .

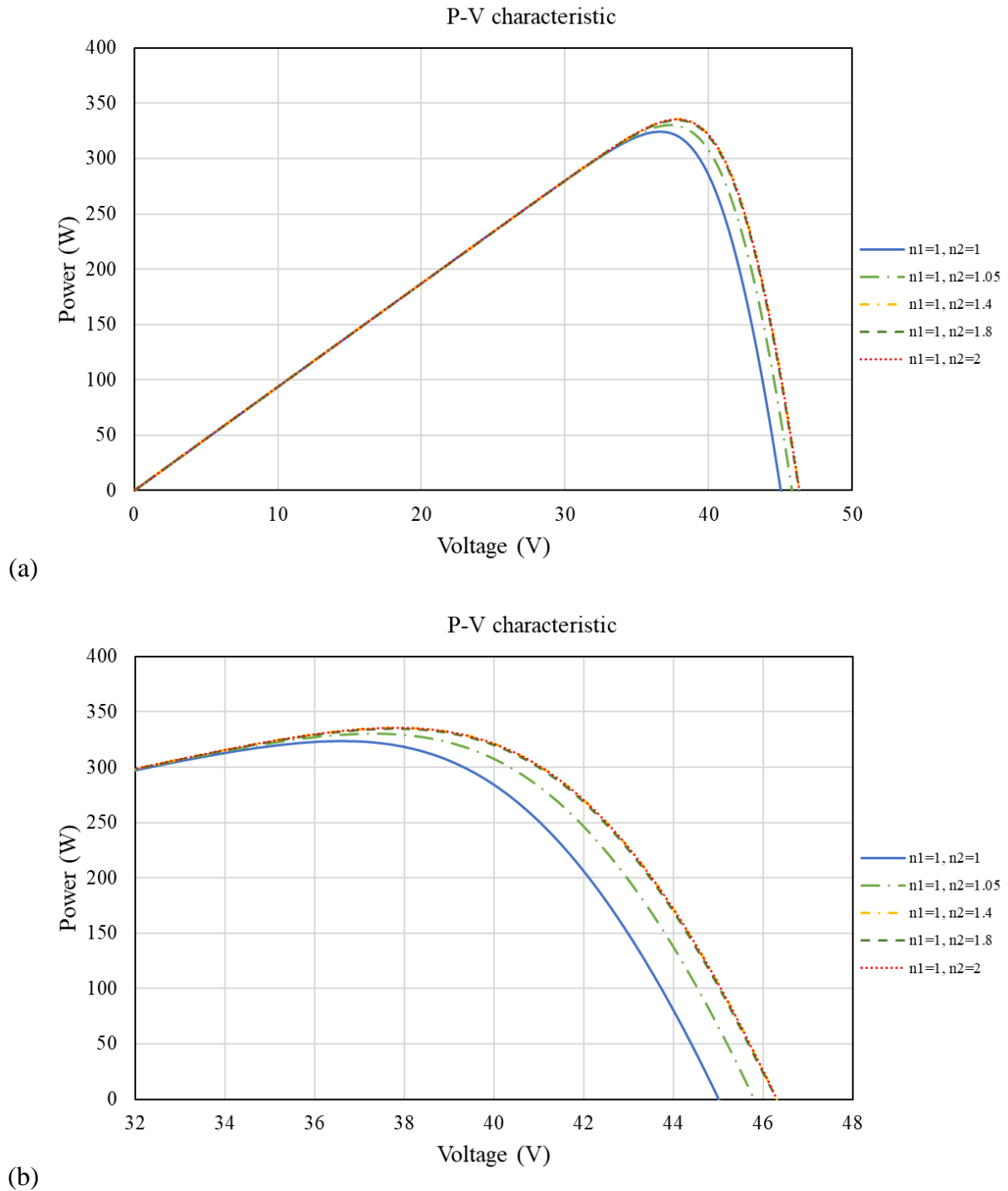


Figure 2-14. P - V curve in response to the change of n_2 : (a) the full range, and (b) enlarged view

2.2.3 Sensitivity of I_{o2}

The effect of size of n_2 on the I - V and the P - V characteristics when $I_{o1} = I_{o2}$ was demonstrated in the previous section, but there is no reason that I_{o1} must equal I_{o2} .

Figure 2-15 and Figure 2-16 show the variation of the I - V and the P - V characteristics in response to the change of I_{o2}/I_{o1} for $n_1 = 1$ and $n_2 = 1.2$ for I_{o1} fixed at 1.3×10^{-10} . A ratio of $I_{o2}/I_{o1} = 0$ is equivalent to the single diode model. A ratio of $I_{o2}/I_{o1} = 1$ was studied in the previous section. Since the second diode has a larger n value, which makes its effect occurs at higher voltage values and be less pronounced than the first diode, only ratios of $I_{o2}/I_{o1} > 1$ (i.e., $I_{o2} > I_{o1}$) are studied. Increasing I_{o2}/I_{o1} will increase its effect of the second diode on the I - V and the P - V characteristics.

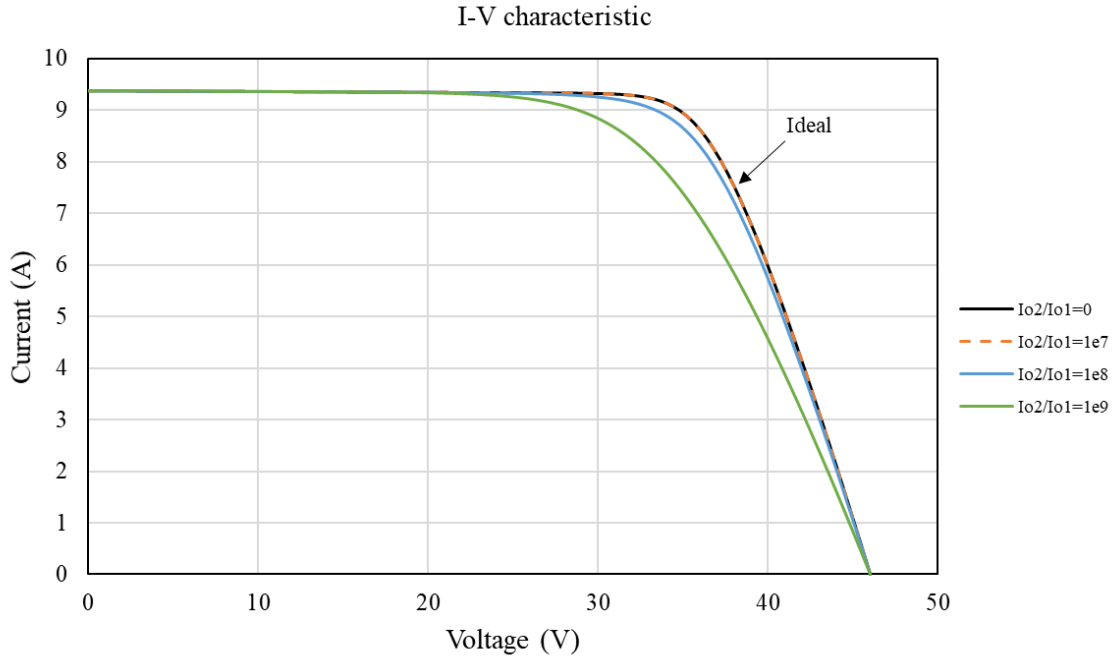


Figure 2-15. I - V curve in response to the change of I_{o2}/I_{o1} for $n_2 = 1.2$

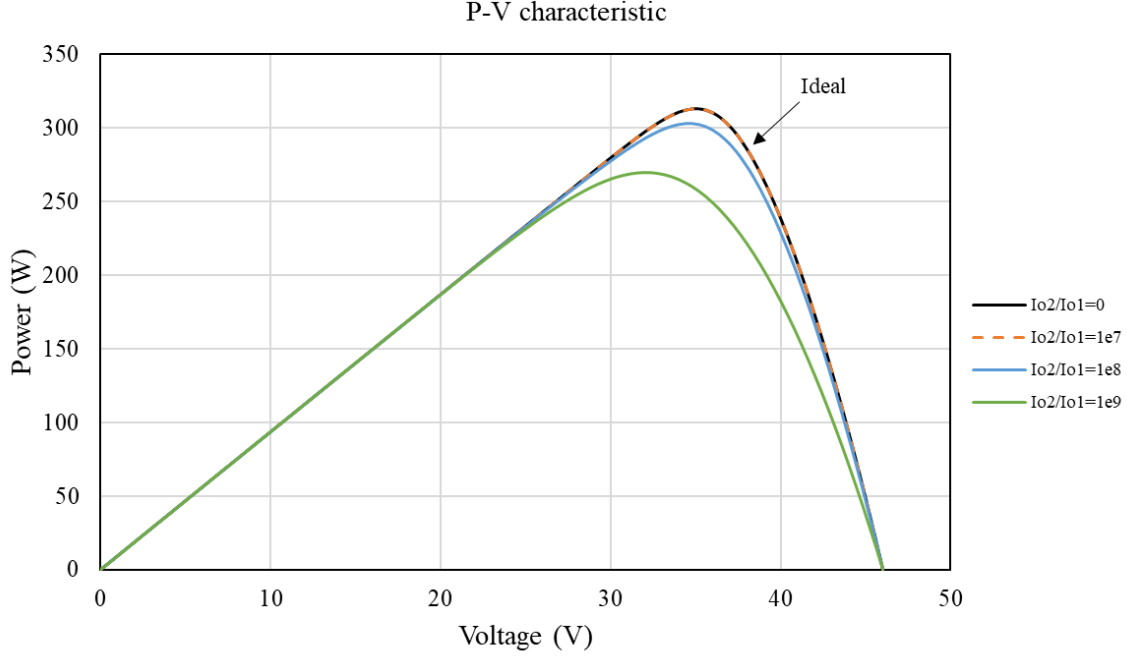


Figure 2-16. P - V curve in response to the change of I_{o2}/I_{o1} for $n_2 = 1.2$

As noted in Section 2.2.2, for monocrystalline solar cells, which are being modelled in the current study, the value of n_1 is assumed to be unity as suggested by most of the previous works, and the value of n_2 varies from 1 to 2. Considering larger values for n_2 , Figure 2-17 and Figure 2-18 show the variation of the I - V and the P - V characteristics in response to the change of I_{o2}/I_{o1} for of $n_1 = 1$ and $n_2 = 1.8$.

As the voltage increases from 0 V to 20 V, the change of I_{o2}/I_{o1} has little impact on the current and the output power. The significance of the ratio of I_{o2} and I_{o1} becomes visible when the voltage is larger than 20 V. For $n_2 = 1.8$, when the ratio of I_{o2} and I_{o1} equals 10^8 , the I - V and the P - V characteristics are almost equivalent to the ideal conditions. However, if the ratio of I_{o2} and I_{o1} continues to increase, for instance, from 10^8 to 10^9 , the effect of the second diode starts to dominate the response. Thus, the larger the value of n_2 the larger ratio of I_{o2} and I_{o1} before the effect of the second diode becomes noticeable. From the figures it is also noteworthy that changing the ratio of I_{o2} and I_{o1} does not change the value of the voltage, V_{OC} , ($I = 0$) or the value of the current, I_{sc} , at $V = 0$.

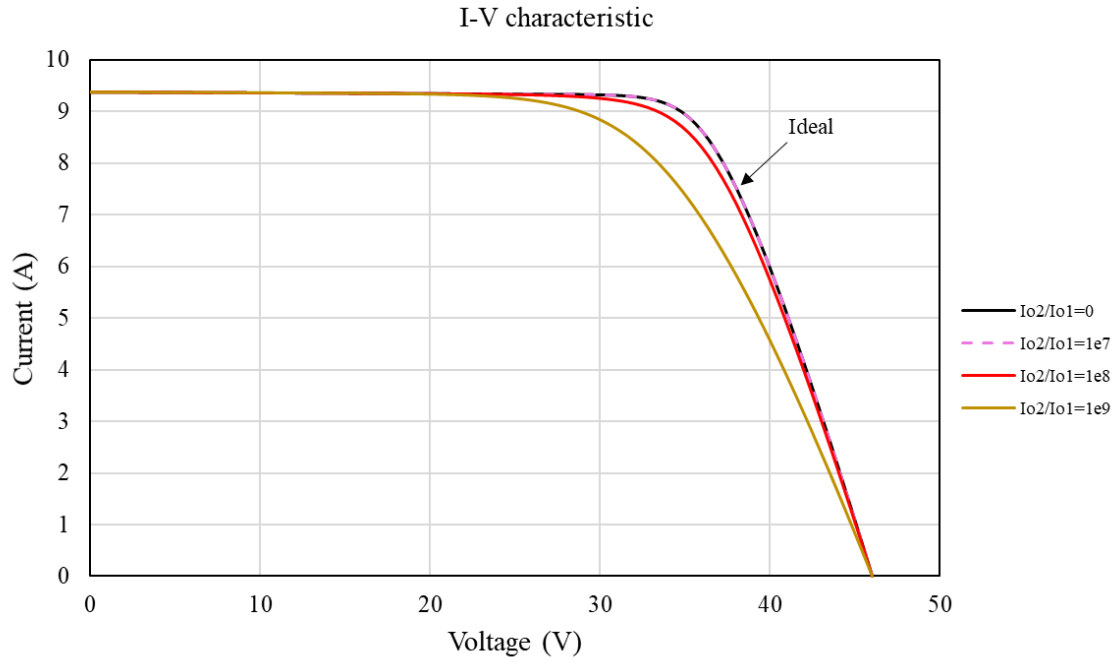


Figure 2-17. I - V curve in response to the change of I_{o2}/I_{o1} for $n_2 = 1.8$

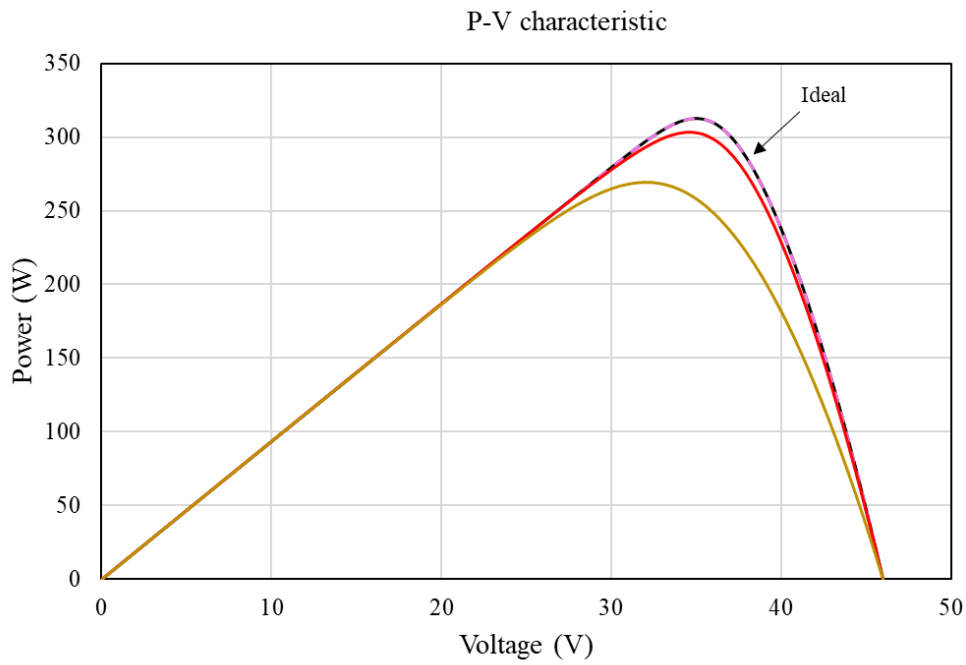


Figure 2-18. P - V curve in response to the change of I_{o2}/I_{o1} for $n_2 = 1.8$

3. OPTIMIZATION OF MODEL PARAMETERS

The single diode model discussed in chapter 2 assumes that the recombination loss in the depletion region is negligible [45]. However, this assumption is not adequate for modeling real solar cells, which have considerable recombination losses. Thus, the double diode model is recommended by previous works to improve the accuracy [44]. The double diode model includes more parameters compared to the single diode model. The primary challenge to apply the double diode model is to obtain the optimum value for each model parameter while maintaining a reasonable computational effort [45]. In this chapter, the governing equations of model parameters in the double diode model are discussed and a method for determining their optimum values is presented.

3.1 Mathematic model

In chapter 2, Eq. (2-13), repeated here for convenience, gives the expression of the current in the double diode model.

$$I = I_{ph} - I_{o1} \left[\exp \frac{q(V + IR_s)}{n_1 N_s kT} - 1 \right] - I_{o2} \left[\exp \frac{q(V + IR_s)}{n_2 N_s kT} - 1 \right] - \frac{V + IR_s}{R_p} \quad (3-1)$$

Using Eq. (2-2), also repeated here for convenience, a more compact form is obtained:

$$V_T = \frac{N_s kT}{q} \quad (3-2)$$

$$I = I_{ph} - I_{o1} \left[\exp \frac{(V + IR_s)}{n_1 V_T} - 1 \right] - I_{o2} \left[\exp \frac{(V + IR_s)}{n_2 V_T} - 1 \right] - \frac{V + IR_s}{R_p} \quad (3-3)$$

In Eq. (3-3), V_T is obtained from known constants, the number of photovoltaic cells in series to form the panel, and the temperature of the panel. Remaining are seven model parameters, I_{ph} , I_{o1} , I_{o2} , n_1 , n_2 , R_s , and R_p that must be determined for proper use of the model. The governing equations of those parameters will be discussed in this section. In previous works, the light-generated current, I_{ph} , has been assumed and shown to be linearly related with irradiation and temperature [55-58] and can be expressed as follows:

$$I_{ph} = (I_{ph,n} + K_I \Delta T) \frac{G}{G_n} \quad (3-4)$$

Where $I_{ph,n}$ is the light-generated current at the nominal condition, i.e., 25 °C and 1000 W/m², K_I is the short-circuit current/temperature coefficient and is provided by the manufacturers, ΔT is the temperature difference between the current condition and the nominal condition, G is the irradiation on the device surface, and G_n is the irradiation at the nominal condition. Since we only have manufacturers data for nominal temperature of 25 °C and thus can only verify our model at this temperature, for this study we will restrict ourselves to operation at 25 °C. Under this constraint, Eq. (3-4) reduces to a linear dependence on irradiation:

$$I_{ph} = I_{ph,n} \frac{G}{G_n} \quad (3-5)$$

In Chapter 2 it was shown that the terms representing the diodes had essentially no effect at I_{sc} , ($V = 0$). Thus at I_{sc} , Eq. (3-3) at reduces to:

$$I_{sc} = I_{ph} - \frac{I_{sc}R_s}{R_p} \quad (3-6)$$

Solving for I_{ph} :

$$I_{ph} = \frac{R_s + R_p}{R_p} I_{sc} \quad (3-7)$$

Since $R_p \gg R_s$, I_{ph} can be approximated by:

$$I_{ph} = I_{sc} \quad (3-8)$$

As noted in Section 2.2.2, most of the previous works have assumed the value of n_1 to be unity and the value of n_2 to be between 1.2 and 2 [46-53] depending upon the semiconductor material used for the photovoltaic. Through simulations McIntosh et al. [45] demonstrates that for silicon diffused junction solar cells (as modeled in this study) depletion-region recombination in silicon solar cells can be modelled using $n_2=1.8$.

Taking the derivative of Eq. (3-3) and evaluating at $I = I_{sc}$,

$$\left. \frac{dI}{dV} \right|_{V=0, I=I_{sc}} = - \frac{\frac{I_{o1}}{n_1 V_T} e^{\frac{I_{sc}R_s}{n_1 V_T}} + \frac{I_{o2}}{n_2 V_T} e^{\frac{I_{sc}R_s}{n_2 V_T}} + \frac{1}{R_p}}{1 + R_s \left[\frac{I_{o1}}{n_1 V_T} e^{\frac{I_{sc}R_s}{n_1 V_T}} + \frac{I_{o2}}{n_2 V_T} e^{\frac{I_{sc}R_s}{n_2 V_T}} + \frac{1}{R_p} \right]} = - \frac{1}{R_p} \quad (3-9)$$

Since all of the terms in in parentheses in the denominator are very small at I_{sc} and R_s is less than 1, the 1 in the denominator dominates. At I_{sc} the $1/R_p$ is much larger that the first two terms in the numerator and dominates the response. Thus, R_p is approximately the negative reciprocal of the slope of the I - V curve at $I = I_{sc}$, which corresponds to the plots in Figure 2-8. Since it is

difficult to obtain the exact slope of the I - V curve at this point, we must determine the slope of the curve near this point as an initial approximation, but the value of R_p will need to be refined.

Taking the derivative of Eq. (3-3) and evaluating at $V = V_{oc}$,

$$\left. \frac{dI}{dV} \right|_{V=V_{oc}, I=0} = - \frac{\frac{I_{o1}}{n_1 V_T} e^{\frac{V_{oc}}{n_1 V_T}} + \frac{I_{o2}}{n_2 V_T} e^{\frac{V_{oc}}{n_2 V_T}} + \frac{1}{R_p}}{1 + R_s \left[\frac{I_{o1}}{n_1 V_T} e^{\frac{V_{oc}}{n_1 V_T}} + \frac{I_{o2}}{n_2 V_T} e^{\frac{V_{oc}}{n_2 V_T}} + \frac{1}{R_p} \right]} \quad (3-10)$$

Since $\frac{I_{o1}}{n_1 V_T} e^{\frac{V_{oc}}{n_1 V_T}}$ dominates the response at $V = V_{oc}$, Eq. (3-10) can be reduced to:

$$\left. \frac{dI}{dV} \right|_{V=V_{oc}, I=0} = - \frac{\frac{I_{o1}}{n_1 V_T} e^{\frac{V_{oc}}{n_1 V_T}}}{1 + R_s \left(\frac{I_{o1}}{n_1 V_T} e^{\frac{V_{oc}}{n_1 V_T}} \right)} \quad (3-11)$$

At $V = V_{oc}$, $\frac{I_{o1}}{n_1 V_T} e^{\frac{V_{oc}}{n_1 V_T}}$ is approximately equal to $I_{sc}/n_1 V_T$. Using this approximation and rearranging Eq. (3-11), the initial value of R_s can be approximated by:

$$R_s = - \left. \frac{dI}{dV} \right|_{V=V_{oc}, I=0} - \frac{n_1 V_T}{I_{sc}} \quad (3-12)$$

In Eq. (3-12), I_{sc} varies as the irradiance changes, thus the second term changes. As a result, the initial value of R_s changes accordingly at different irradiance.

In Section 2.2.3 the effect of I_{o1} and I_{o2} on the I - V curve were shown. Since I_{o1} and I_{o2} greatly affect the value and slope of the I - V curve between the maximum power point and $V = V_{oc}$, two equations and two unknowns can be developed by looking at the I - V curves. Initially it was desired to use the values and the slope of the I - V curve at the maximum power point, but accurate values for the slope at the maximum power point were difficult to obtain from manufacturer's data. Instead, the value of the I - V curve at the maximum power point and at V_{oc} were used to approximate I_{o1} and I_{o2} . Evaluating Eq. (3-3) at the maximum power point where the current and voltage are defined as I_{mp} and V_{mp} :

$$I_{mp} = I_{ph} - I_{o1}(A_{mp} - 1) - I_{o2}(B_{mp} - 1) - \frac{V_{mp} + I_{mp}R_s}{R_p} \quad (3-13)$$

Where:

$$A_{mp} = \exp \left(\frac{V_{mp} + I_{mp}R_s}{n_1 V_T} \right) \quad (3-14)$$

$$B_{mp} = \exp \left(\frac{V_{mp} + I_{mp}R_s}{n_2V_T} \right) \quad (3-15)$$

Evaluating Eq. (3-3) at $V = V_{oc}$, $I = 0$:

$$0 = I_{ph} - I_{o1}(A_{oc} - 1) - I_{o2}(B_{oc} - 1) - \frac{V_{oc}}{R_p} \quad (3-16)$$

Where:

$$A_{oc} = \exp \left(\frac{V_{oc}}{n_1V_T} \right) \quad (3-17)$$

$$B_{oc} = \exp \left(\frac{V_{oc}}{n_2V_T} \right) \quad (3-18)$$

The value of I_{o1} and I_{o2} can be easily found by solving Eq. (3-13), Eq. (3-14), Eq. (3-15), Eq. (3-16), Eq. (3-17) and Eq. (3-18) together. Together with Eq. (3-8), Eq. (3-9), and Eq. (3-12), the initial values of the seven model parameters *i.e.*, I_{ph} , I_{o1} , I_{o2} , n_1 , n_2 , R_s , and R_p , can be solved.

3.2 Newton-Raphson method

The previous section presents a method to obtain I using seven model parameters, but the accuracy can be further improved through an iterative process. Among all iterative techniques, the Newton-Raphson method is one of the most widely used methods due to its efficiency and accuracy.

The Newton-Raphson method is a root-finding algorithm which produces successively better approximations to the roots [62]. Figure 3-1 visualizes the iterative process for a single-variable function $f(x)$. The iterative process starts with an initial guess x_0 , which should be sufficiently close to the root. At $x = x_0$, $f(x_0)$ and $f'(x_0)$ are computed, respectively. $f(x_0)$ represents the value on the $f(x)$ curve when $x = x_0$, whereas $f'(x_0)$ is the slope of $f(x)$ at $(x_0, f(x_0))$. The next better approximation is the point at which the tangent line to $f(x)$ at $(x_0, f(x_0))$ crosses the x axis. If this better approximation is referred to as x_1 , then x_1 can be determined by the following equation:

$$x_1 = x_0 - \frac{f(x_0)}{f'(x_0)} \quad (3-19)$$

Once the value of x_1 is known, $f(x_1)$ and $f'(x_1)$ can be found consequently. Similarly, the next better approximation, *i.e.*, x_2 , can be found by using the same approach. After n th succeeding iterations, the $(n+1)^{th}$ better approximation can be expressed as follows [62]:

$$x_{n+1} = x_n - \frac{f(x_n)}{f'(x_n)} \quad (3-20)$$

This process is repeated until the desired accuracy is met.

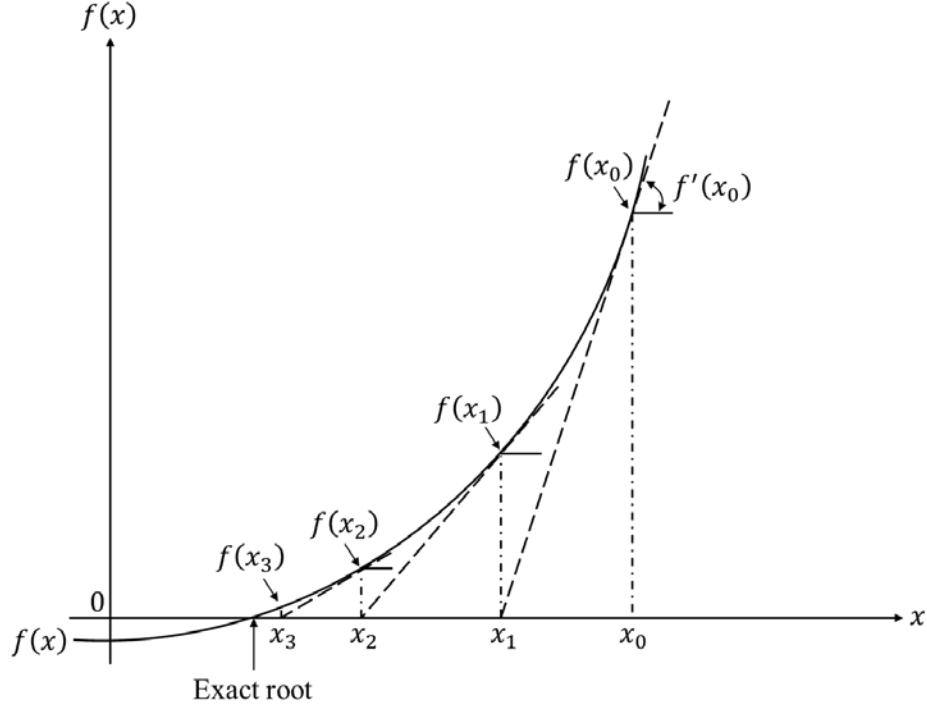


Figure 3-1. Visualization of the Newton-Raphson method

The current study applies the Newton-Raphson method to numerically solve Eq. (2-13) for I . To enable the iterative process, Eq. (2-13) is modified as follows:

$$f(I) = I_{ph} - I_{o1} \left[\exp\left(\frac{V + IR_s}{n_1 V_T}\right) - 1 \right] - I_{o2} \left[\exp\left(\frac{V + IR_s}{n_2 V_T}\right) - 1 \right] - \frac{V + IR_s}{R_p} - I \quad (3-21)$$

The expression of $f'(I)$ can be found by taking the derivative of $f(I)$:

$$f'(I) = -I_{o1} \frac{R_s}{n_1 V_T} \exp\left(\frac{V + IR_s}{n_1 V_T}\right) - I_{o2} \frac{R_s}{n_2 V_T} \exp\left(\frac{V + IR_s}{n_2 V_T}\right) - \frac{R_s}{R_p} - 1 \quad (3-22)$$

After n^{th} succeeding iterations, the better approximation to Eq. (3-21) can be expressed as follows:

$$I_{n+1} = I_n - \frac{f(I_n)}{f'(I_n)} \quad (3-23)$$

3.3 Determination of model parameters

As mentioned in the previous section, the optimum values of the model parameters of the double diode model are numerically obtained through an iterative process as shown in Figure 3-2.. The main idea behind the method is to match the calculated maximum power point at (V_{mp}, I_{mp}) with the measured maximum power point through an iterative process. The calculated maximum power point can be expressed as follows:

$$\begin{aligned}
 P_{max,m} &= P_{max,e} \\
 &= V_{mp} \left\{ I_{ph} - I_{o1} \left[\exp \left(\frac{V_{mp} + I_{mp} R_s}{n_1 V_T} \right) - 1 \right] \right. \\
 &\quad \left. + I_{o2} \left[\exp \left(\frac{V_{mp} + I_{mp} R_s}{n_2 V_T} \right) - 1 \right] - \frac{V_{mp} + R_s I_{mp}}{R_p} \right\}
 \end{aligned} \tag{3-24}$$

Rearranging Eq. (3-24) and solving for R_p , yields:

$$\begin{aligned}
 R_p &= \frac{V_{mp} + R_s I_{mp}}{V_{mp} I_{pv} - V_{mp} \left\{ I_{o1} \left[\exp \left(\frac{V_{mp} + I_{mp} R_s}{n_1 V_T} \right) - 1 \right] + I_{o2} \left[\exp \left(\frac{V_{mp} + I_{mp} R_s}{n_2 V_T} \right) - 1 \right] - \right\} - P_{max},} \tag{3-25}
 \end{aligned}$$

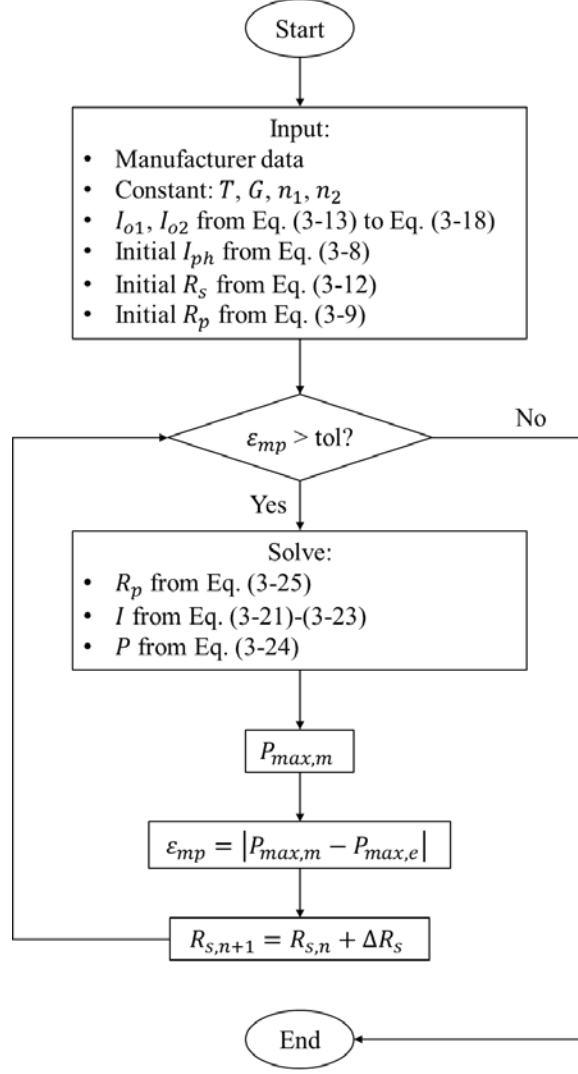


Figure 3-2. Flowchart of the iterative process

At the beginning of the iterative process, manufacturer data and model constants are provided to the program. The manufacturer data includes I_{sc} , V_{oc} , I_{mp} , V_{mp} , K_I , K_V , and N_S . The maximum power point from the manufacturer can be found by:

$$P_{max,e} = V_{mp} I_{mp} \quad (3-26)$$

The condition to continue or end the process is based on the error between the calculated maximum power point and the measured maximum power point:

$$\varepsilon_{mp} = |P_{max,m} - P_{max,e}| \quad (3-27)$$

If $\varepsilon_{mp} < tol$, the solutions of the model reach the desired accuracy and the iterative process is stopped. The solutions and the corresponding I - V and P - V curves are given as the model outputs.

On the other hand, if $\varepsilon_{mp} > tol$, the solutions of the model are still not the optimum and better approximations are required. The new R_p is obtained by computing Eq. (3-25). Then, the new I is calculated from the Newton-Raphson method shown in Eq. (3-21)-Eq. (3-23). Finally, the new ε_{mp} is evaluated using Eq. (3-27) and the value of R_s is increased by a fixed increment. If the new $\varepsilon_{mp} < tol$, the iterative process is ended. Otherwise, the aforementioned process repeats.

4. RESULTS

In this chapter, the performance of two PV modules is modeled using the double diode model (discussed in Chapter 2) and the model parameter optimization (discussed in Chapter 3). The two PV modules are selected from two manufacturers, which are Trinasolar and SolarEdge. Based on the datasheet provided by the manufacturers, the optimum model parameters are obtained. Then, the I - V and P - V characteristics of each PV module are modeled and compared with the manufacturer's measurements. Finally, the effect of irradiance on the performance of the PV module is discussed.

4.1 Comparison with Trinasolar

4.1.1 Manufacturer datasheet

Figure 4-1 (a) and (b) show the dimensions of the PV module TSM-PD14 developed by Trinasolar, one of the global leading providers for PV modules and smart energy solution. The PV module contains 72 cells, and the power output ranges from 320 W to 340 W with maximum 17.5% efficiency. The I - V and P - V characteristics of the PV module under different irradiances are shown in Figure 4-2 and Figure 4-3.

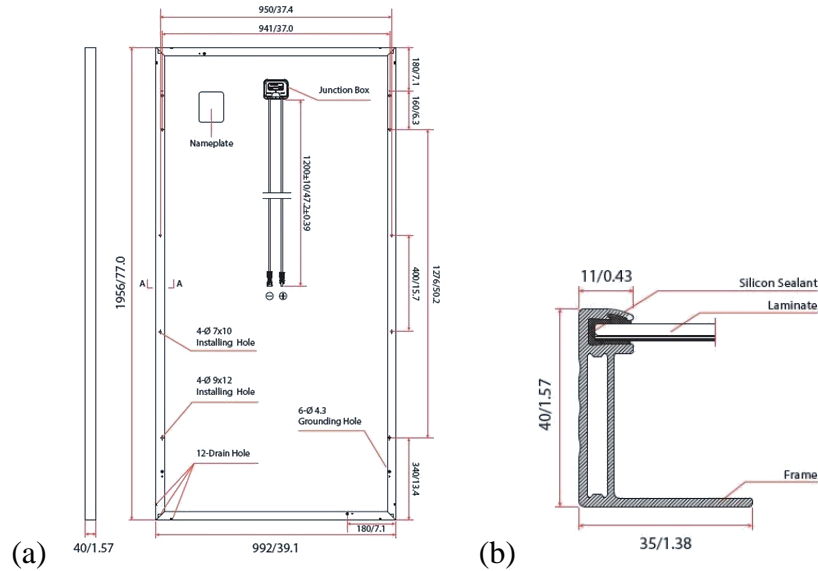


Figure 4-1. Dimensions of the PV module TSM-PD14 (mm/inch) [63]: (a) back view, and (b) cross-section A-A.

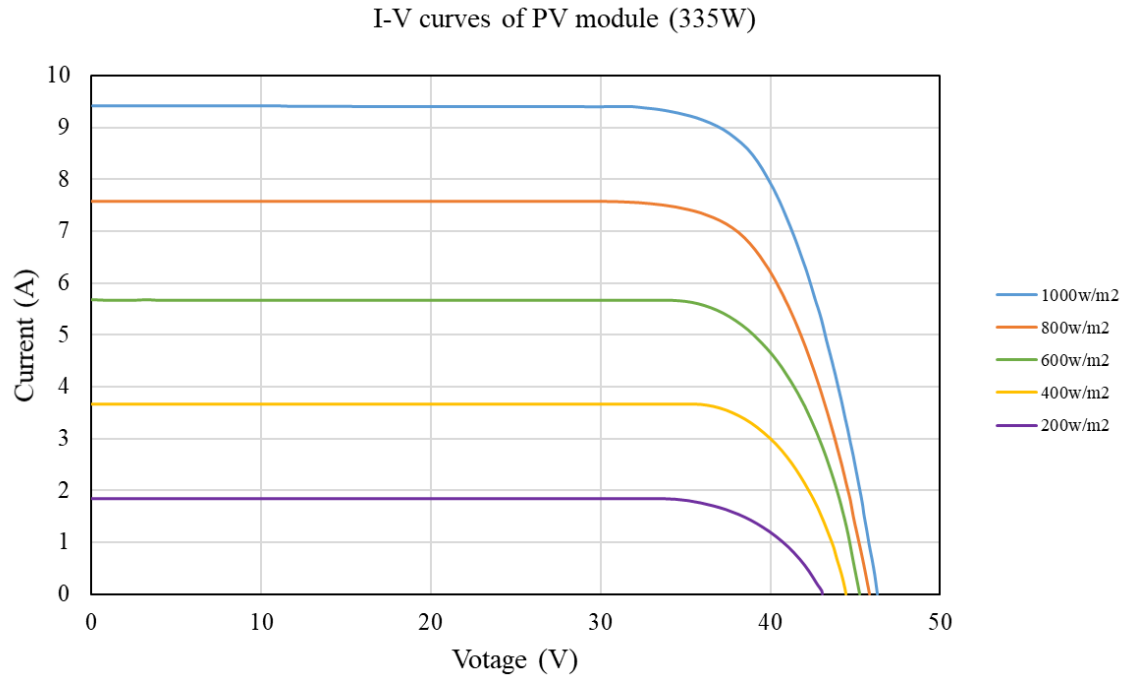


Figure 4-2. *I-V* curves of the PV module TSM-PD14 (335W) [63]

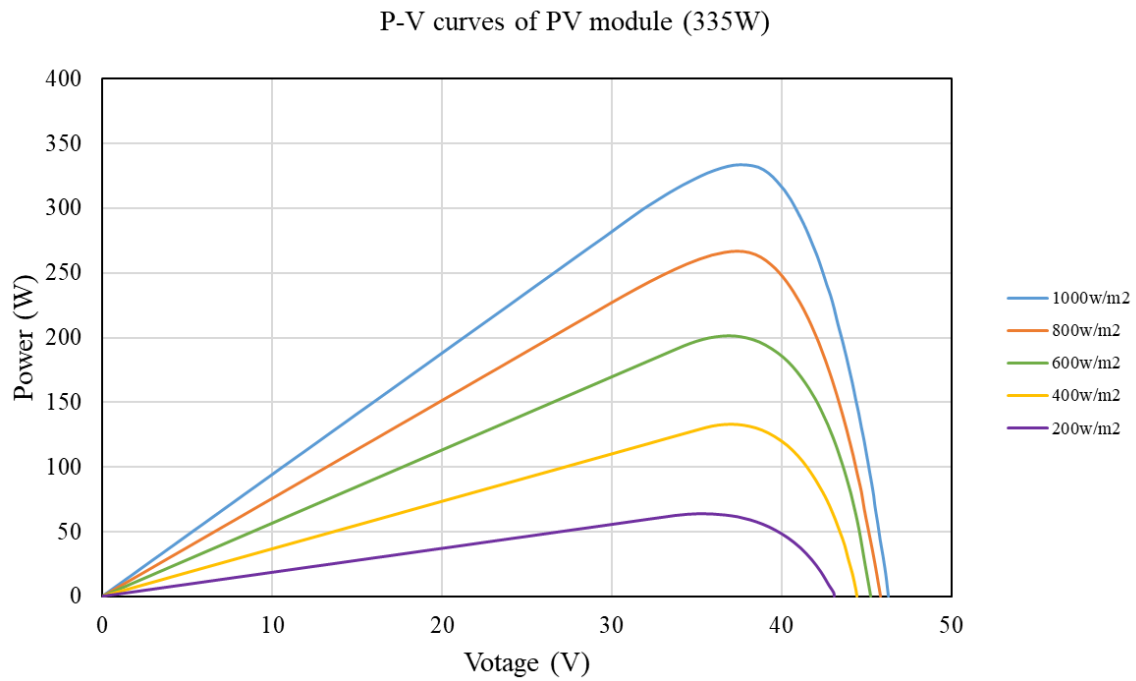


Figure 4-3. *P-V* curves of the PV module TSM-PD14 (335W) [63]

Table 4-1 lists the electric data, including short-circuit current, open-circuit voltage, maximum power point current and voltage, and temperature coefficients, of the PV module TSM-PD14 (335W) under different irradiances at the standard test environment. The number of series cells is 72.

Table 4-1 Electrical data of the PV module TSM-PD14 (335W) [63]

	Irradiance (w/m ²)				
	1000	800	600	400	200
Short-circuit current I_{SC} (A)	9.39	7.57	5.67	3.66	1.85
Open-circuit voltage V_{OC} (V)	46.3	45.85	45.24	44.47	43.08
Maximum power current (A)	8.91	7.31	5.42	3.54	1.81
Maximum power voltage (V)	37.6	37.39	37.19	37.39	35.18
MPP (W)	335	266.83	201.53	132.62	63.74
Temperature coefficient of V_{OC} (V/C)	$K_v = -0.32\%$				
Temperature coefficient of I_{SC} (A/C)	$K_i = 0.05\%$				
Number of series cells	$N_s = 72$				

4.1.2 Optimized model parameter

The optimized model parameters for the double diode model under different irradiances are tabulated in Table 4-2. The optimized model parameters were obtained using the manufactures' datasheet listed in Table 4-1 and the equations developed in Chapter 3. The resistance R_s and R_p were then refined using the Newton-Raphson method described in Chapter 3. The diode ideality factors, *i.e.* n_1 and n_2 , were set to 1 and 1.8 respectively.

As shown in Table 4-2, the final values of R_p and R_s are neither constantly ascending nor descending as the irradiance decreases from 1000 W/m² to 200 W/m², as demonstrated by Orioli and Gangi [64]. The final value of R_p is at least one order of magnitude larger than its initial value, while the final value of R_s is near the initial estimated value as expected.

Table 4-2 Summary of the optimized model parameters for the PV module TSM-PD14 (335W)

	Irradiance (w/m ²)				
	1000	800	600	400	200
R_p initial value	1327	7073	1752	5885	17144
R_p final value	6.09×10^4	6.44×10^3	5.79×10^4	542	1.15×10^6
R_s initial value	0.10	0.410	0.354	0.489	0.96
R_s final value	0.172	0.411	0.398	0.608	0.994
$I_{o1} \times 10^{-10}$	0.863	1.242	1.305	0.112	0.110
$I_{o2} \times 10^{-5}$	0.273	3.647	2.427	-0.131	-0.162
Diode ideality factor	$n_1 = 1, n_2 = 1.8, p = 2.8$				

4.1.3 I - V and P - V characteristics

Figure 4-4 and Figure 4-5 compare the manufacturer's measured I - V and P - V characteristics with the calculated characteristics, using Eq. (2-13), in the standard test condition. The calculated model parameters presented in the previous section were used as the inputs to calculate the characteristics. The calculated I - V and P - V characteristics show good agreement with the manufacturer's measurements. The current model can accurately predict the I - V and P - V characteristics within 1% relative difference especially at the maximum power point, at which the system is desired to work.

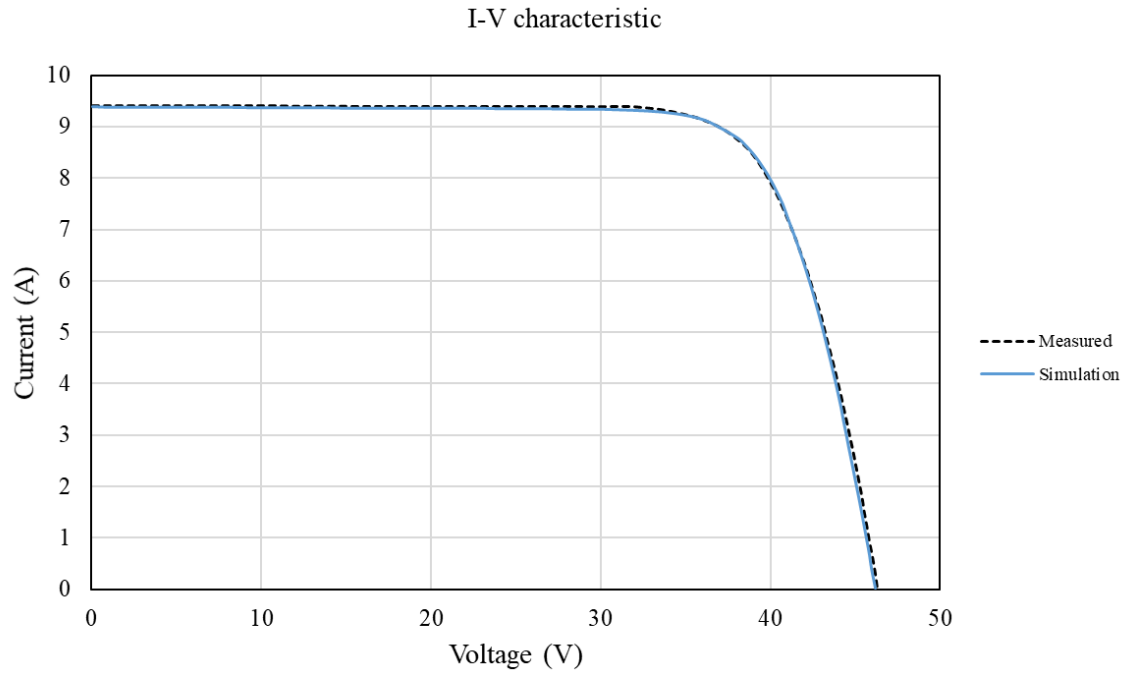


Figure 4-4. Comparison between the measured I - V characteristic and the calculated characteristic in the standard test condition

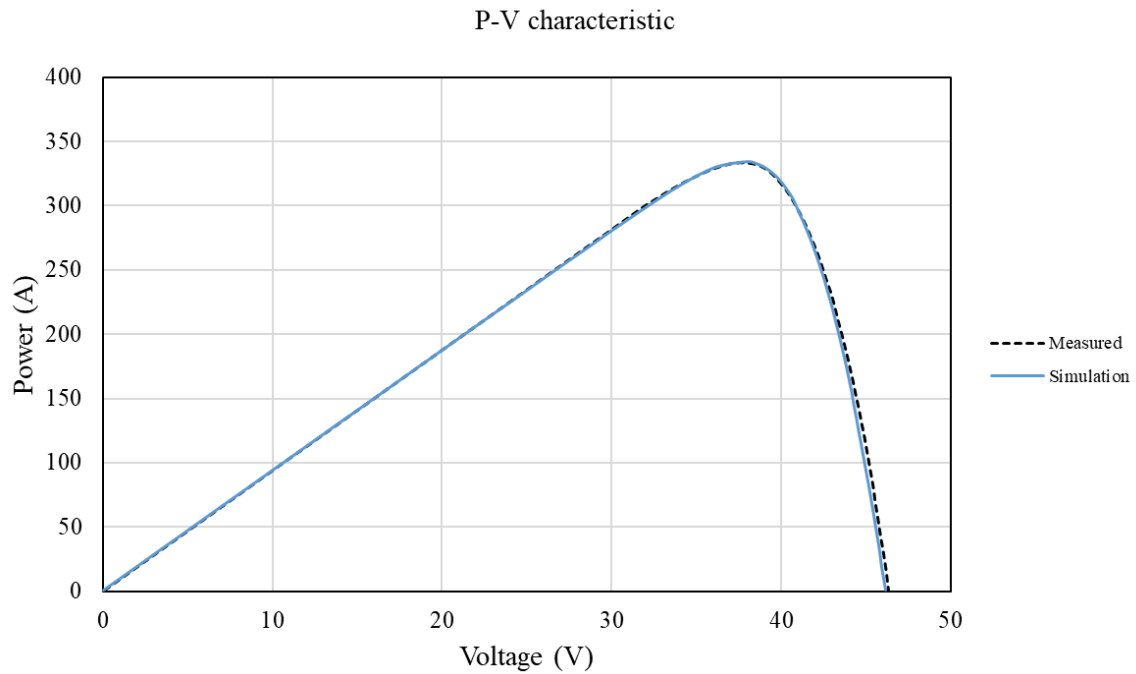


Figure 4-5. Comparison between the measured P - V characteristic and the calculated characteristic in the standard test condition

4.1.4 Effect of irradiance

Once the PV panel is installed, the I - V and P - V characteristics are mostly affected by the solar irradiance. The previous calculation assumes that the irradiance is constant and is kept at 1000 W/m^2 . Solar irradiance at any location varies due to cloud cover, time of day, and time of the year. Figure 4-6 shows the U.S. annual average daily solar irradiance; which can be seen varies with location. In order to study the effect of irradiance on the performance of the PV panel, 5 irradiance values, *i.e.* 1000 W/m^2 , 800 W/m^2 , 600 W/m^2 , 400 W/m^2 , and 200 W/m^2 , were selected. Model parameters from Table 4-2 were used for the calculations.

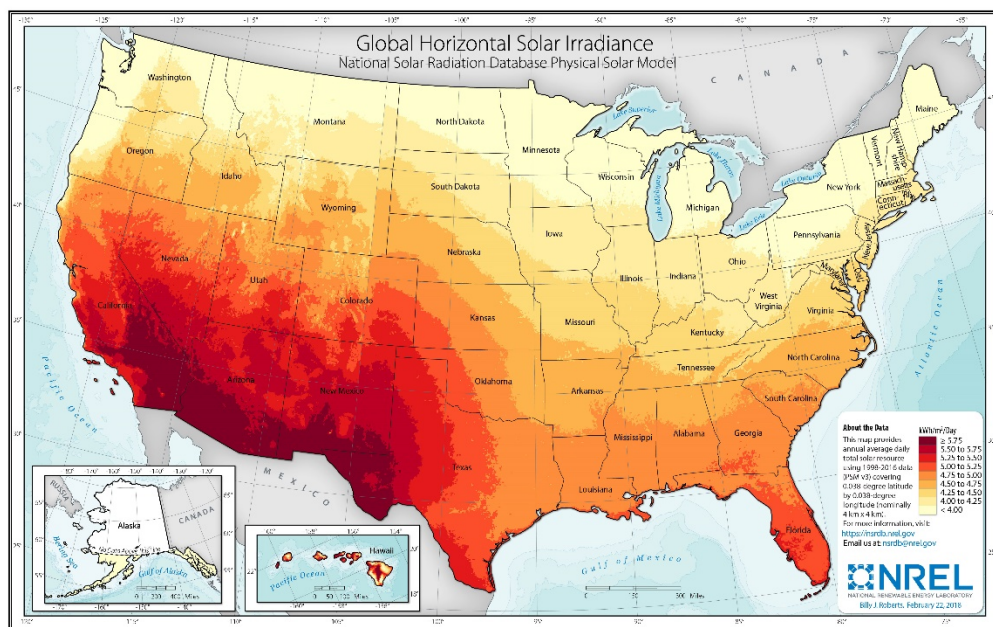


Figure 4-6. U.S. annual global horizontal irradiance [65]

Figure 4-7 and Figure 4-8 compare manufacturer's the measured I - V and P - V characteristics with the calculated characteristics as the irradiance varies from 1000 W/m^2 to 200 W/m^2 . Both the characteristics calculated using the initial parameters and the parameter values updated using the Newton-Raphson method match well with the measured characteristics even when the irradiance changes. Higher accuracy can be seen at voltages before the maximum power point regardless of the irradiance and the calculation method. The modeled characteristics directly calculated from the initial parameter values noticeably deviate from the manufacturer's measured values after the maximum power point, but the accuracy is significantly improved if the parameters updated using

the Newton-Raphson method, with the input from the calculated initial values, is applied to the model.

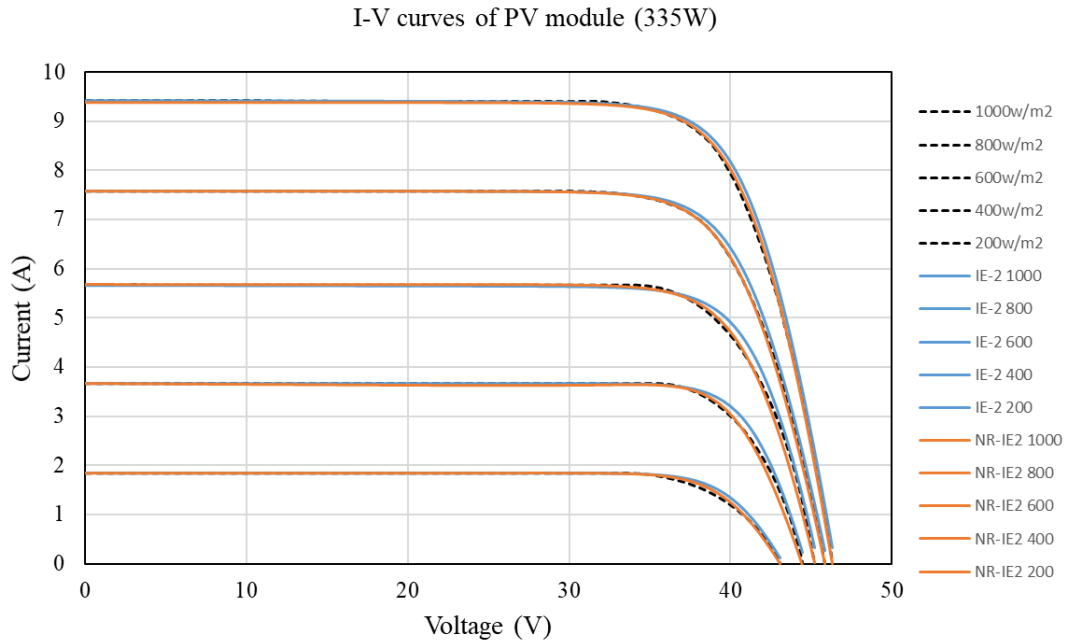


Figure 4-7. Comparison between the measured I - V characteristic of the PV module TSM-PD14 and the calculated characteristic at different irradiances

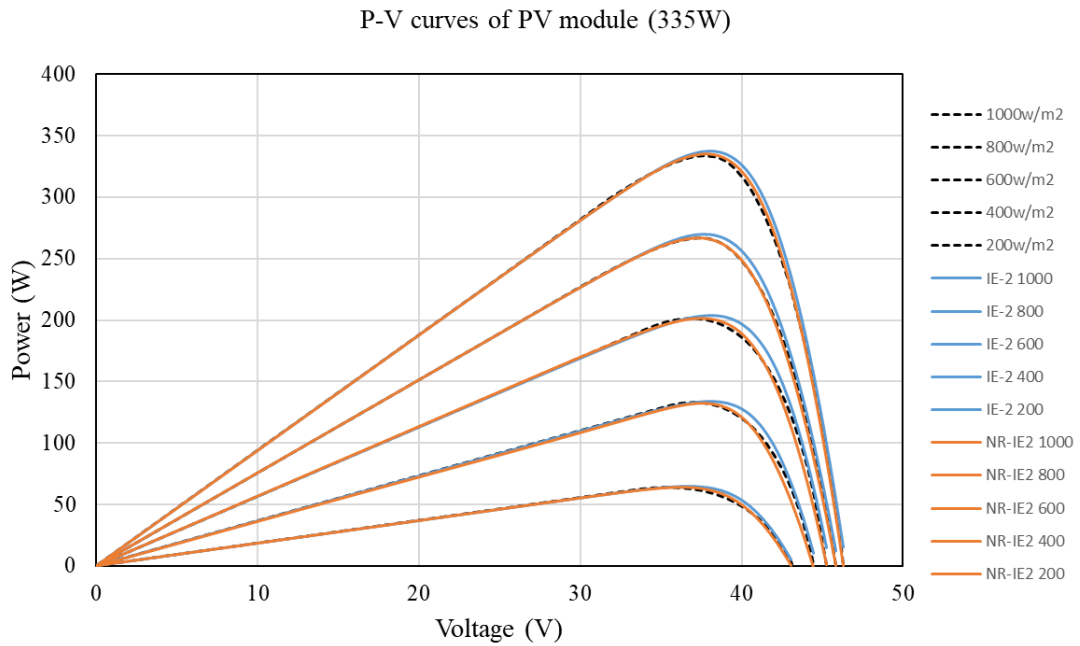


Figure 4-8. Comparison between the measured P - V characteristic of the PV module TSM-PD14 and the calculated characteristic at different irradiances

4.2 Comparison with SolarEdge

4.2.1 Manufacturer datasheet

Figure 4-9 (a) and (b) show the dimensions of the PV module SPV300-60MMJ developed by SolarEdge, another world leader in smart energy solutions. The PV module contains 60 cells, and the designed power output is 300 W with maximum 18.3% efficiency. The module is also integrated with a solar power optimizer, which optimizes energy output by constantly tracking the maximum power point and mitigates all types of modules mismatch-loss including manufacturing tolerance and partial shading. The I - V and P - V characteristics of the PV module under different irradiances are shown in Figure 4-10 and Figure 4-11. It is worth mentioning that the change of the slope near the maximum power point is not smooth on both of the manufacturer's plots.

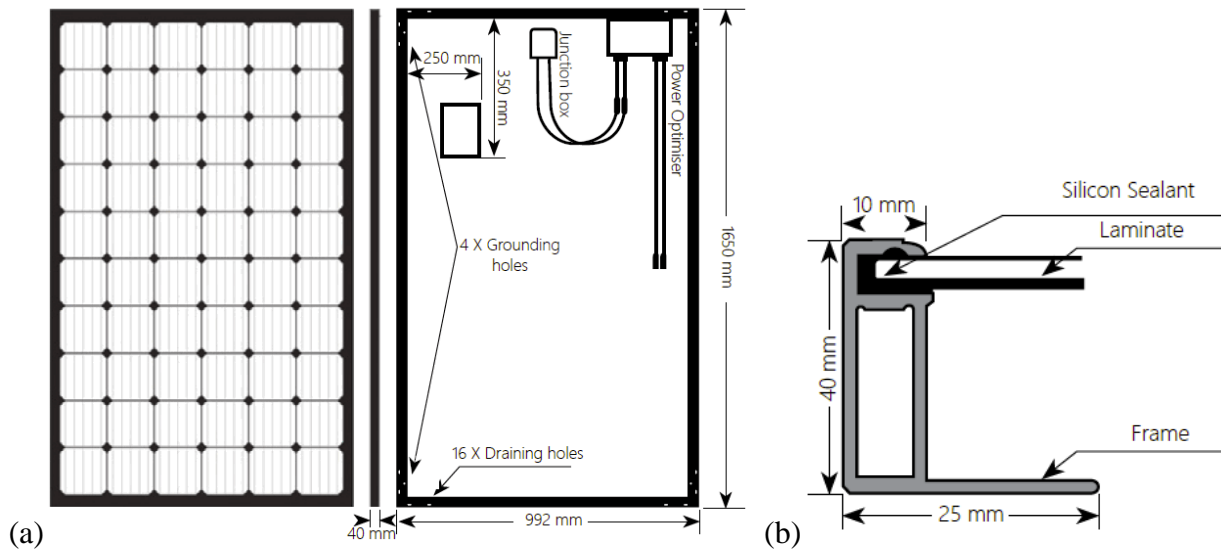


Figure 4-9. Dimensions of the PV module SPV300-60MMJ [66]: (a) front view, side view, and back view, and (b) cross-section view.

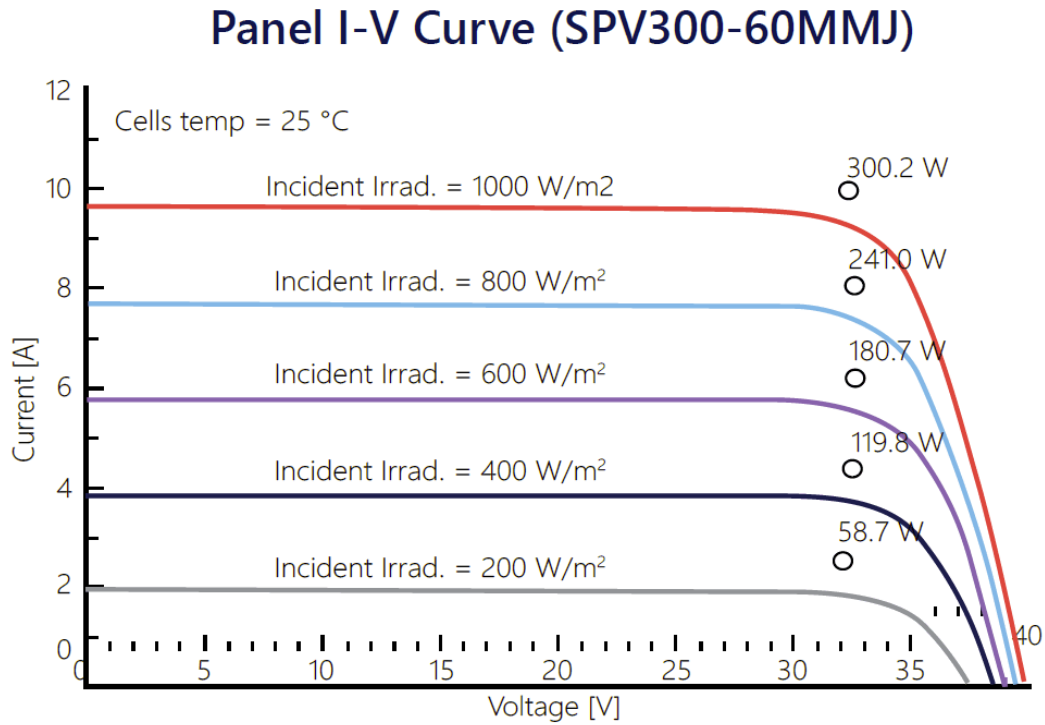


Figure 4-10. *I-V* curves of the PV module SPV300-60MMJ [66]

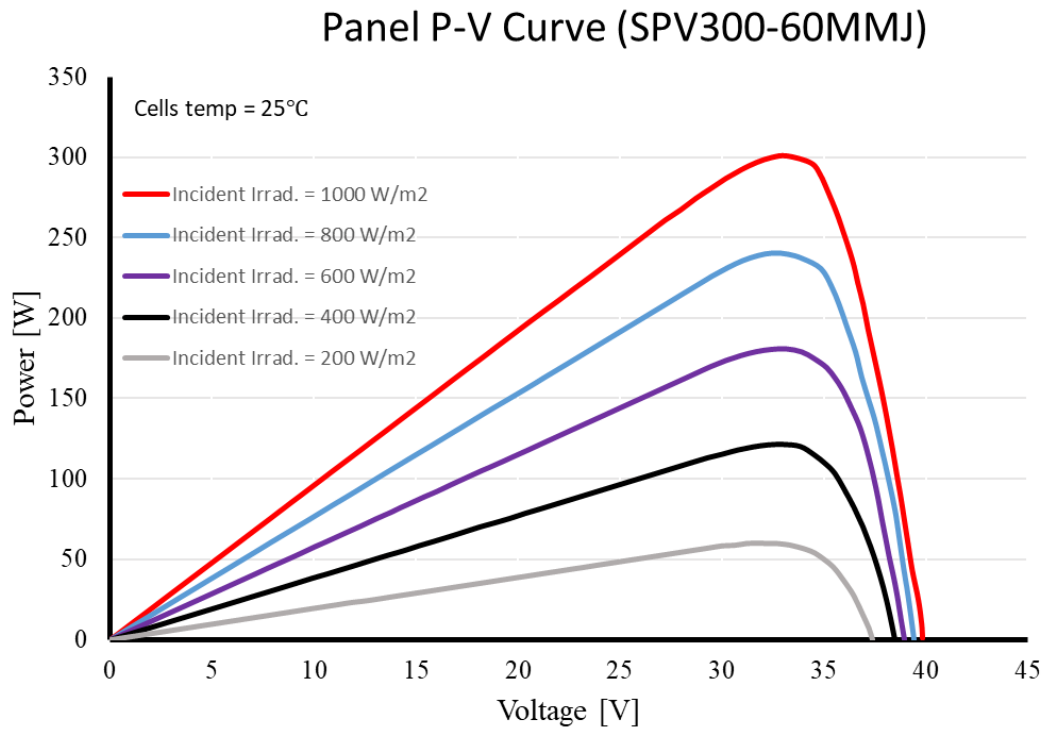


Figure 4-11. *P-V* curves of the PV module SPV300-60MMJ [66]

Table 4-3 lists the electric data, including short-circuit current, open-circuit voltage, maximum power point current and voltage, and temperature coefficients, of the PV module SPV300-60MMJ under different irradiances at the standard test environment. The number of series cells is 60.

Table 4-3 Electrical data of the PV module SPV300-60MMJ [66]

	Irradiance (w/m ²)				
	1000	800	600	400	200
Short-circuit current I_{SC} (A)	9.64	7.66	5.74	3.84	1.95
Open-circuit voltage V_{OC} (V)	39.75	39.41	38.94	38.46	37.40
Maximum power Current (A)	9.2	7.39	5.45	3.67	1.89
Maximum power Voltage (V)	32.62	32.48	33.15	33.00	31.75
MPP (W)	300	240.28	180.66	121.05	60.12
Temperature coefficient of V_{OC} (V/C)	$K_v = -0.29\%$				
Temperature coefficient of I_{SC} (A/C)	$K_i = 0.04\%$				
Number of series cells	$N_s = 60$				

4.2.2 Optimized model parameter

The optimized model parameters for the double diode model under different irradiances are tabulated in Table 4-4. The optimized model parameters were obtained using the Newton-Raphson method described in chapter 3 with the manufacturers' datasheet listed in Table 4-3. At the beginning of the iteration, the initial values of R_s and R_p were obtained from Chapter 3. The diode ideality factors, *i.e.* n_1 and n_2 , were set to 1 and 1.8 respectively.

Similar to section 4.1, the final value of R_p is at least one order of magnitude larger than its initial value, while the final value of R_s is near the initial estimated value as expected.

Table 4-4 Summary of the optimized model parameters for the PV module SPV300-60MMJ [66]

	Irradiance (w/m ²)				
	1000	800	600	400	200
R_p initial value	1010	1508	835	4053	1877
R_p final value	1.918×10^4	2.202×10^4	1.362×10^5	3.942×10^5	8.311×10^3
R_s initial value	0.3197	0.2979	0.3107	0.4253	0.6352
R_s final value	0.3267	0.3100	0.3407	0.4383	0.7992
$I_{o1} \times 10^{-10}$	0.6936	0.6656	0.7085	0.6814	4.197
$I_{o2} \times 10^{-5}$	-0.1112	-5.365	-7.317	-8.095	-2.928
Diode ideality factor	$n_1 = 1, n_2 = 1.8, p = 2.8$				

4.2.3 I - V and P - V characteristics

Figure 4-12 and Figure 4-13 compare the measured manufacturer's I - V and P - V characteristics with the calculated characteristics, using Eq. (2-13) in the standard test condition. The calculated model parameters presented in the previous section were used as the inputs to calculate the characteristics. The calculated I - V and P - V characteristics show good agreement with the measurements. The current model can accurately predict the I - V and P - V characteristics within 1% relative difference especially at the maximum power point, at which the system is desired to work. As noted earlier the I - V and P - V plots from the manufacturer's data sheet were not very smooth near the maximum power point.

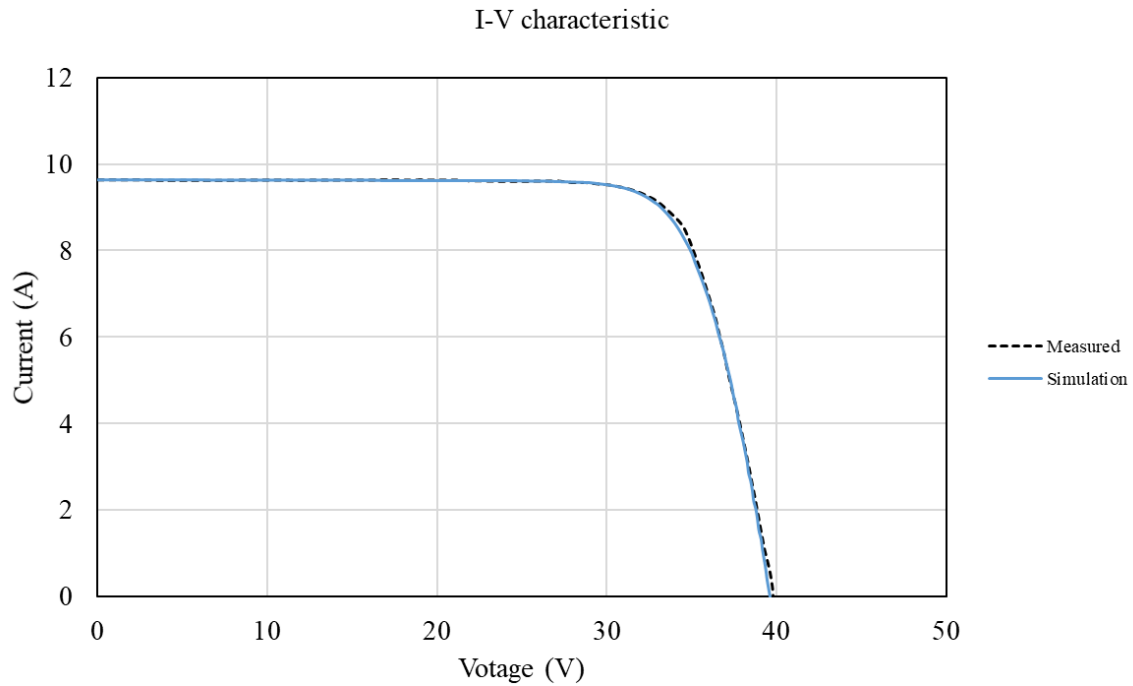


Figure 4-12. Comparison between the measured I - V characteristic and the calculated characteristic in the standard test condition

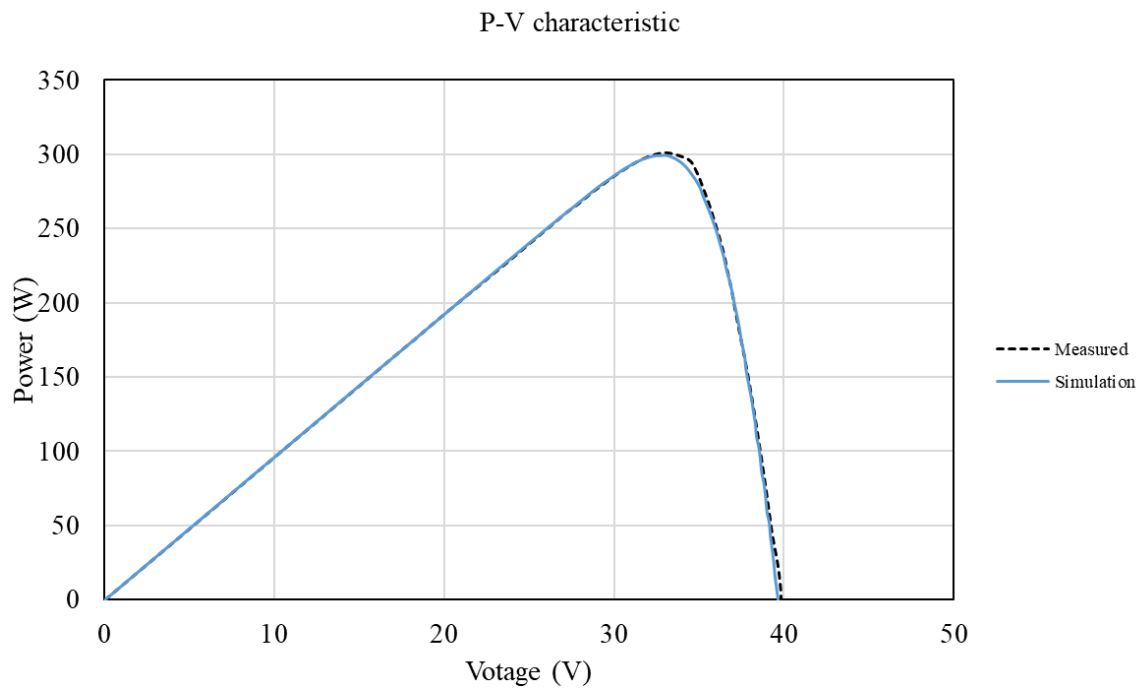


Figure 4-13. Comparison between the measured P - V characteristic and the calculated characteristic in the standard test condition

4.2.4 Effect of irradiance

Figure 4-14 and Figure 4-15 compare the measured I - V and P - V characteristics of the PV module SPV300-60MMJ with the characteristics calculated using the initial values and the Newton-Raphson method as the irradiance varies from 1000 W/m^2 to 200 W/m^2 . The calculated characteristics match reasonably with the manufacturer's measured characteristics under different irradiances. The predicted characteristics from both methods show some discrepancies near the maximum power point regardless of the irradiance. In addition, unlike the previous section, the values of I_{o2} under different irradiances are all negative, as shown in Table 4-4, which is physically unrealistic, but does produce models that match the manufacturers curves more closely. It is possible to force the value of I_{o2} to be positive by reducing the value of n_1 . However, the accuracy of the prediction does not improve even with the positive I_{o2} . One of the possible reasons is due to the insufficient number of accurate measured data points near the maximum power point in the manufacturer's datasheet, as shown in Figure 4-10 and Figure 4-11. If more data points are provided, the prediction accuracy may be potentially improved.

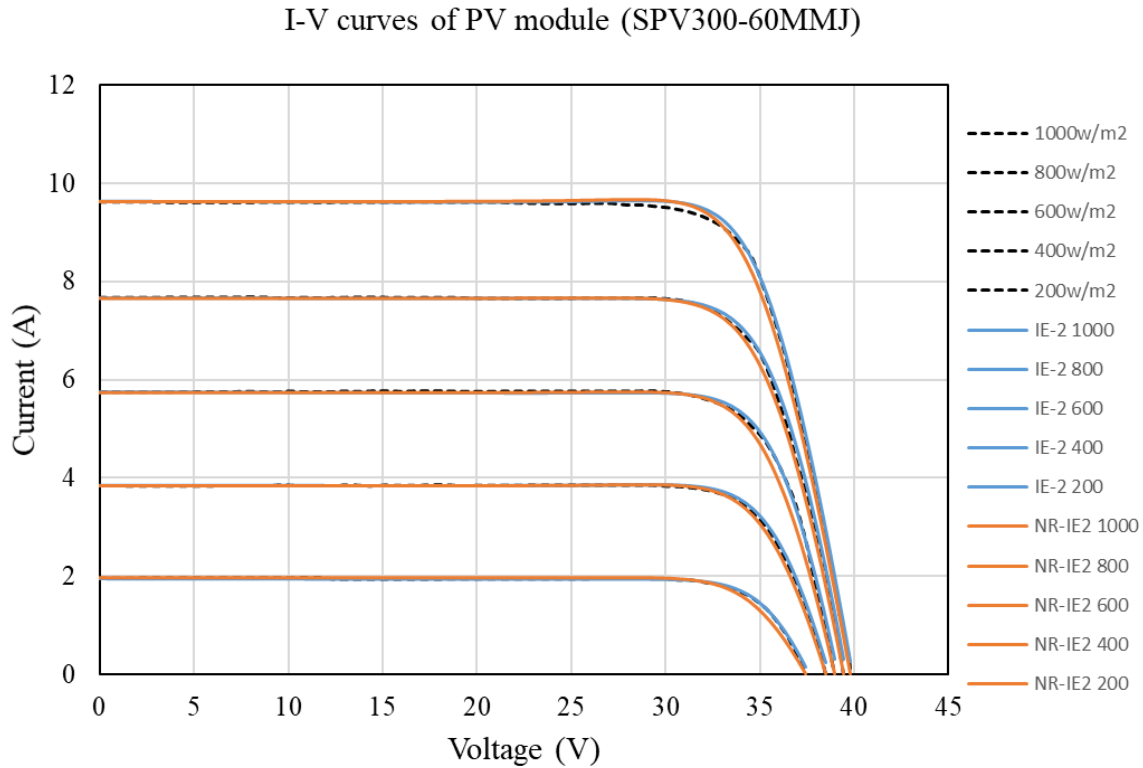


Figure 4-14. Comparison between the measured I - V characteristic of the PV module SPV300-60MMJ and the calculated characteristic at different irradiances

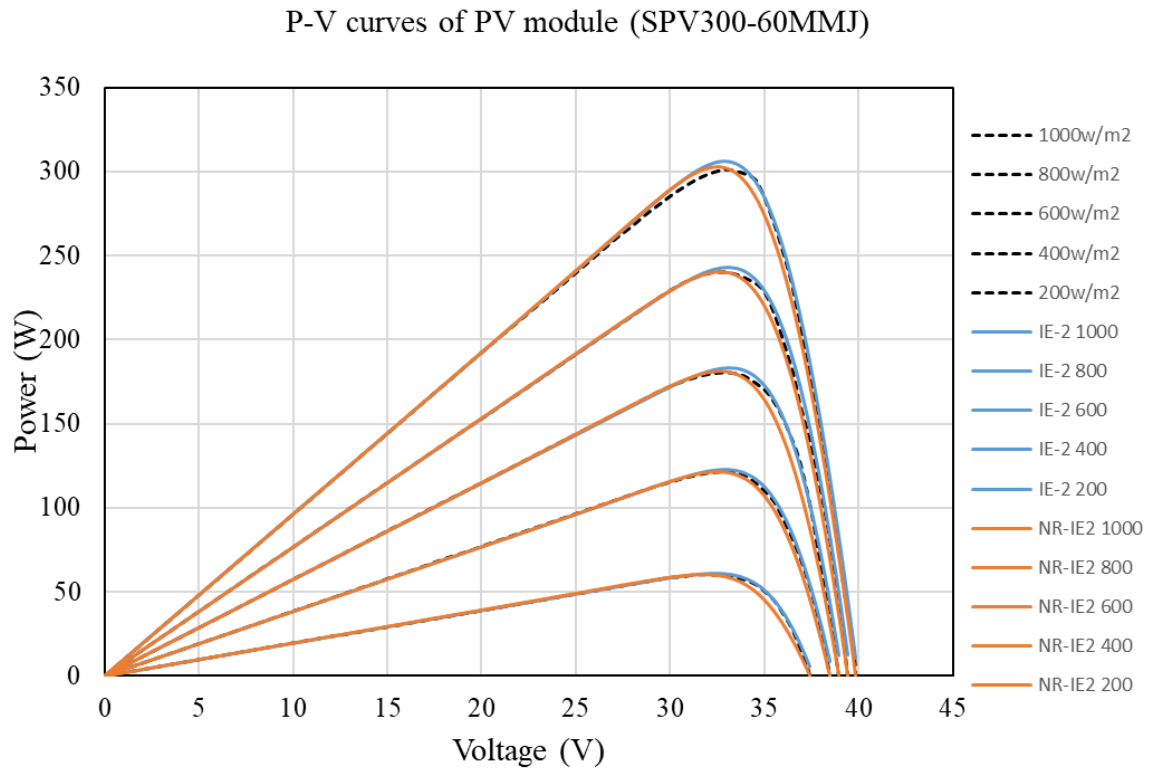


Figure 4-15. Comparison between the measured P - V characteristic of the PV module SPV300-60MMJ and the calculated characteristic at different irradiances

5. CONCLUSION

5.1 Conclusions

Several equivalent circuit models such as the single diode and the double diode model have been proposed by previous researchers and were discussed in the current study. The single diode model is relatively simple and requires an insignificant amount of computational time, but it would fail if the recombination loss were substantial. The double diode model includes more parameters to represent the recombination loss, but this improvement in accuracy comes at the cost of adding more parameters to the model. The primary challenge to applying the double diode model is obtaining the optimum value for each model parameter so as to obtain an accurate model, while maintaining a reasonable computational effort.

The current study investigated the effect of each term in the double diode model. It then proposed a method to obtain an initial estimate for each of the seven model parameters from data provided by the manufacturer. Using these initial estimated parameters as inputs, the Newton-Raphson method was applied to improve parameter estimates and prediction accuracy. The performance of two PV modules from different manufacturers was then modeled using the initial parameter estimates and the Newton-Raphson updated parameters. Both were compared to the manufacturers data.

The modeled I - V and P - V characteristics of the PV module TSM-PD14 using the initial parameter estimation method noticeably deviated from the measured values after the maximum power point, but the accuracy of the model was significantly improved when the initial parameter estimates were updated using the Newton-Raphson method.

On the other hand, the modeled I - V and P - V characteristics of the PV module SPV300-60MMJ using both the initial parameter estimation and the parameters updated using the Newton-Raphson method both show some discrepancies near the maximum power point regardless of the irradiance. In addition, the value of I_{o2} becomes negative, which is physically impossible, regardless of the irradiances. Reducing n_1 would make I_{o2} positive but increase the inaccuracies in the model. One possible cause of the errors is an insufficient number of measured data points near the maximum power point in the manufacturer's datasheet.

5.2 Future work

Future research could include the following aspects:

(1) The current study predicts negative I_{o2} under certain circumstances, but the negative values are not physically possible. Future research can improve the current model by constraining the value of I_{o2} to be positive while varying n_1 and n_2 and updating I_{o1} and I_{o2} in addition to R_s and R_p .

(2) In the current study, I_{o1} and I_{o2} were determined by evaluating I at $V = V_{mp}$ and $V = V_{oc}$. Initially it was desired to use I and the slope of I at $V = V_{mp}$. This was not possible due to the insufficient number of the measured data points near the maximum power point in the manufacturers' datasheet. Using the manufacturer data curves, the slope of the I - V curve varied greatly between points near the maximum power point, and values of the slope were very sensitive to small changes in the estimates of the data points. Future research can improve the current model by evaluating the derivative of I at the maximum power point with sufficient number of the measured data points.

(3) Future research can evaluate and compare the accuracy of different iterative methods.

REFERENCES

- [1] The Part Played by Labour in the Transition from Ape to Man. (2020, November 11). Retrieved December 30, 2020, from https://en.wikipedia.org/wiki/The_Part_Played_by_Labour_in_the_Transition_from_Ape_to_Man
- [2] Layton, B. E. (2008). A comparison of energy densities of prevalent energy sources in units of joules per cubic meter. *International Journal of Green Energy*, 5(6), 438-455.
- [3] U.S. Energy Information Administration. (2021, May 20). Renewable energy explained. <https://www.eia.gov/energyexplained/renewable-sources/>
- [4] U.S. Energy Information Administration. (2021, March 18). Electricity explained. <https://www.eia.gov/energyexplained/electricity/electricity-in-the-us.php>
- [5] Kajihara, A., & Harakawa, A. T. (2005, December). Model of photovoltaic cell circuits under partial shading. In 2005 IEEE International Conference on Industrial Technology (pp. 866-870). IEEE.
- [6] Bingöl, O., & Özkaya, B. (2018). Analysis and comparison of different PV array configurations under partial shading conditions. *Solar Energy*, 160, 336-343.
- [7] U.S. Energy Information Administration. (2021, March 26). Solar explained-photovoltaics and electricity. <https://www.eia.gov/energyexplained/solar/photovoltaics-and-electricity.php>
- [8] Wikipedia contributors. Photovoltaic effect. Wikipedia, The Free Encyclopedia. August 9, 2021, 10:44 UTC. Available at: https://en.wikipedia.org/w/index.php?title=Photovoltaic_effect&oldid=1037903081.
- [9] File:From a solar cell to a PV system.svg. (2021, May 27). *Wikimedia Commons, the free media repository*. Retrieved 22:31, September 23, 2021 from https://commons.wikimedia.org/w/index.php?title=File:From_a_solar_cell_to_a_PV_system.svg&oldid=565272772.
- [10] Solarbotics.net. (2002, February 28). Solar cells-performance and use. http://solarbotics.net/starting/200202_solar_cells/200202_solar_cell_use.html
- [11] Roundy, S., Wright, P. K., & Rabaey, J. M. (2003). Energy scavenging for wireless sensor networks. In *Norwell* (pp. 45-47).

- [12] Ishaque, K., Salam, Z., & Taheri, H. (2011). Simple, fast and accurate two-diode model for photovoltaic modules. *Solar energy materials and solar cells*, 95(2), 586-594.
- [13] Tan, Y. T., Kirschen, D. S., & Jenkins, N. (2004). A model of PV generation suitable for stability analysis. *IEEE Transactions on energy conversion*, 19(4), 748-755.
- [14] Kajihara, A., & Harakawa, A. T. (2005, December). Model of photovoltaic cell circuits under partial shading. In *2005 IEEE International Conference on Industrial Technology* (pp. 866-870). IEEE.
- [15] “Photovoltaics: Solar Electricity and Solar Cells in Theory and Practice.” Solar Server. Ed. Julia Winter. Heindl Server GmbH, 2010. Web. Feb. 2011. <http://www.solarserver.com/>.
- [16] Xiao, W., Dunford, W. G., & Capel, A. (2004, June). A novel modeling method for photovoltaic cells. In *2004 IEEE 35th Annual Power Electronics Specialists Conference (IEEE Cat. No. 04CH37551)* (Vol. 3, pp. 1950-1956). IEEE.
- [17] Walker, G. (2001). Evaluating MPPT converter topologies using a MATLAB PV model. *Journal of Electrical & Electronics Engineering, Australia*, 21(1), 49-55.
- [18] Khouzam, K., Ly, C., Koh, C. K., & Ng, P. Y. (1994, December). Simulation and real-time modelling of space photovoltaic systems. In *Proceedings of 1994 IEEE 1st World Conference on Photovoltaic Energy Conversion-WCPEC (A Joint Conference of PVSC, PVSEC and PSEC)* (Vol. 2, pp. 2038-2041). IEEE.
- [19] Liu, S., & Dougal, R. A. (2002). Dynamic multiphysics model for solar array. *IEEE Transactions on Energy Conversion*, 17(2), 285-294.
- [20] Chegaar, M., Ouennoughi, Z., & Hoffmann, A. (2001). A new method for evaluating illuminated solar cell parameters. *Solid-state electronics*, 45(2), 293-296.
- [21] Sera, D., Teodorescu, R., & Rodriguez, P. (2007, June). PV panel model based on datasheet values. In *2007 IEEE international symposium on industrial electronics* (pp. 2392-2396). IEEE.
- [22] Villalva, M. G., Gazoli, J. R., & Ruppert Filho, E. (2009). Comprehensive approach to modeling and simulation of photovoltaic arrays. *IEEE Transactions on power electronics*, 24(5), 1198-1208.
- [23] Ahmad, T., Sobhan, S., & Nayan, M. F. (2016). Comparative analysis between single diode and double diode model of PV cell: concentrate different parameters effect on its efficiency. *Journal of Power and Energy Engineering*, 4(3), 31-46.

- [24] Matagne, E., Chenni, R., & El Bachtiri, R. (2007, April). A photovoltaic cell model based on nominal data only. In *2007 International conference on power engineering, energy and electrical drives* (pp. 562-565). IEEE.
- [25] Elshatter, T. F., Elhaggee, M. E., Aboueldahab, Elkousry, A. A. (1997). Fuzzy modeling and simulation of photovoltaic system. In proceedings of the 14th European Photovoltaic Solar Energy Conference.
- [26] Balzani, M., & Reatti, A. (2005, July). Neural network based model of a PV array for the optimum performance of PV system. In *Research in Microelectronics and Electronics, 2005 PhD* (Vol. 2, pp. 123-126). IEEE.
- [27] Mellit, A., Benghanem, M., & Kalogirou, S. A. (2007). Modeling and simulation of a stand-alone photovoltaic system using an adaptive artificial neural network: Proposition for a new sizing procedure. *Renewable energy*, 32(2), 285-313.
- [28] Karatepe, E., Boztepe, M., & Colak, M. (2006). Neural network based solar cell model. *Energy conversion and management*, 47(9-10), 1159-1178.
- [29] Syafaruddin, Karatepe, E., & Hiyama, T. (2010). Development of real-time simulator based on intelligent techniques for maximum power point controller of photovoltaic system. *International Journal of Innovative Computing Information and Control*, 6(4), 1623-1642.
- [30] Gow, J. A., & Manning, C. D. (1999). Development of a photovoltaic array model for use in power-electronics simulation studies. *IEE Proceedings-Electric Power Applications*, 146(2), 193-200.
- [31] Gow, J. A., & Manning, C. D. (1996). Development of a model for photovoltaic arrays suitable for use in simulation studies of solar energy conversion systems.
- [32] Chowdhury, S., Taylor, G. A., Chowdhury, S. P., Saha, A. K., & Song, Y. H. (2007, September). Modelling, simulation and performance analysis of a PV array in an embedded environment. In *2007 42nd International Universities Power Engineering Conference* (pp. 781-785). IEEE.
- [33] Hovinen, A. (1994). Fitting of the solar cell IV-curve to the two diode model. *Physica Scripta*, 1994(T54), 175.
- [34] Hyvarinen, J., & Karila, J. (2003, May). New analysis method for crystalline silicon cells. In *3rd World Conference on Photovoltaic Energy Conversion, 2003. Proceedings of* (Vol. 2, pp. 1521-1524). IEEE.

- [35] Kurobe, K. I., & Matsunami, H. (2005). New two-diode model for detailed analysis of multicrystalline silicon solar cells. *Japanese journal of applied physics*, 44(12R), 8314.
- [36] Nishioka, K., Sakitani, N., Kurobe, K. I., Yamamoto, Y., Ishikawa, Y., Uraoka, Y., & Fuyuki, T. (2003). Analysis of the temperature characteristics in polycrystalline Si solar cells using modified equivalent circuit model. *Japanese journal of applied physics*, 42(12R), 7175.
- [37] Nishioka, K., Sakitani, N., Uraoka, Y., & Fuyuki, T. (2007). Analysis of multicrystalline silicon solar cells by modified 3-diode equivalent circuit model taking leakage current through periphery into consideration. *Solar energy materials and solar cells*, 91(13), 1222-1227.
- [38] Salam, Z., Ishaque, K., & Taheri, H. (2010, December). An improved two-diode photovoltaic (PV) model for PV system. In 2010 Joint International Conference on Power Electronics, Drives and Energy Systems & 2010 Power India (pp. 1-5). IEEE.
- [39] Ishaque, K., Salam, Z., & Taheri, H. (2011). Accurate MATLAB simulink PV system simulator based on a two-diode model. *Journal of Power Electronics*, 11(2), 179-187.
- [40] Marrekchi, A., Sallem, S., Kammoun, M. A., & Tina, G. M. (2015, March). A new five parameters estimation method for two-diode model of PV module. In IREC2015 The Sixth International Renewable Energy Congress (pp. 1-6). IEEE.
- [41] Duong, M. Q., Nguyen, H. H., Leva, S., Mussetta, M., Sava, G. N., & Costinas, S. (2016, June). Performance analysis of a 310Wp photovoltaic module based on single and double diode model. In 2016 International Symposium on Fundamentals of Electrical Engineering (ISFEE) (pp. 1-6). IEEE.
- [42] Nguyen, H. H., & Duong, M. Q. (2016, November). High-performance coordination for accurate Matlab Simulink PV module simulator based on a two-diode model. In 2016 IEEE International Conference on Sustainable Energy Technologies (ICSET) (pp. 379-383). IEEE.
- [43] Gupta, S., Tiwari, H., Fozdar, M., & Chandna, V. (2012, March). Development of a two diode model for photovoltaic modules suitable for use in simulation studies. In 2012 Asia-Pacific Power and Energy Engineering Conference (pp. 1-4). IEEE.
- [44] Elbaset, A. A., Ali, H., & Abd-El Sattar, M. (2014). Novel seven-parameter model for photovoltaic modules. *Solar energy materials and Solar cells*, 130, 442-455.
- [45] Sah, C. T., Noyce, R. N., & Shockley, W. (1957). Carrier generation and recombination in pn junctions and pn junction characteristics. *Proceedings of the IRE*, 45(9), 1228-1243.

- [46] Chan, D. S., & Phang, J. C. (1987). Analytical methods for the extraction of solar-cell single-and double-diode model parameters from IV characteristics. *IEEE Transactions on Electron devices*, 34(2), 286-293.
- [47] Enebish, N., Agchbayar, D., Dorjkhand, S., Baatar, D., & Ylemj, I. (1993). Numerical analysis of solar cell current-voltage characteristics. *Solar energy materials and solar cells*, 29(3), 201-208.
- [48] Hovinen, A. (1994). Fitting of the solar cell IV-curve to the two diode model. *Physica Scripta*, 1994(T54), 175.
- [49] Gow, J. A., & Manning, C. D. (1999). Development of a photovoltaic array model for use in power-electronics simulation studies. *IEE Proceedings-Electric Power Applications*, 146(2), 193-200.
- [50] Haouari-Merbah, M., Belhamel, M., Tobias, I., & Ruiz, J. M. (2005). Extraction and analysis of solar cell parameters from the illuminated current–voltage curve. *Solar Energy Materials and Solar Cells*, 87(1-4), 225-233.
- [51] Hejri, M., Mokhtari, H., Azizian, M. R., Ghandhari, M., & Söder, L. (2014). On the parameter extraction of a five-parameter double-diode model of photovoltaic cells and modules. *IEEE Journal of Photovoltaics*, 4(3), 915-923.
- [52] Masmoudi, F., Salem, F. B., & Derbel, N. (2016, March). Single and double diode models for conventional mono-crystalline solar cell with extraction of internal parameters. In *2016 13th International Multi-Conference on Systems, Signals & Devices (SSD)* (pp. 720-728). IEEE.
- [53] Sallem, S., Marrekchi, A., Kammoun, S., & Kammoun, M. B. A. (2016). Multi-PV technologies method for parameters estimation of two-diode model. *The European Physical Journal Plus*, 131(12), 1-10.
- [54] Würfel, P., & Würfel, U. (2016). *Physics of solar cells: from basic principles to advanced concepts*. John Wiley & Sons.
- [55] Sera, D., Teodorescu, R., & Rodriguez, P. (2007, June). PV panel model based on datasheet values. In *2007 IEEE international symposium on industrial electronics* (pp. 2392-2396). IEEE.
- [56] De Soto, W., Klein, S. A., & Beckman, W. A. (2006). Improvement and validation of a model for photovoltaic array performance. *Solar energy*, 80(1), 78-88.

- [57] Kou, Q., Klein, S. A., & Beckman, W. A. (1998). A method for estimating the long-term performance of direct-coupled PV pumping systems. *Solar Energy*, 64(1-3), 33-40.
- [58] Driesse, A., Harrison, S., & Jain, P. (2007, June). Evaluating the effectiveness of maximum power point tracking methods in photovoltaic power systems using array performance models. In *2007 IEEE Power Electronics Specialists Conference* (pp. 145-151). IEEE.
- [59] Villalva, M. G., Gazoli, J. R., & Ruppert Filho, E. (2009). Comprehensive approach to modeling and simulation of photovoltaic arrays. *IEEE Transactions on power electronics*, 24(5), 1198-1208.
- [60] Glass, M. C. (1996, August). Improved solar array power point model with SPICE realization. In *IECEC 96. Proceedings of the 31st Intersociety Energy Conversion Engineering Conference* (Vol. 1, pp. 286-291). IEEE.
- [61] Ortiz-Rivera, E. I., & Peng, F. Z. (2005, June). Analytical model for a photovoltaic module using the electrical characteristics provided by the manufacturer data sheet. In *2005 IEEE 36th Power Electronics Specialists Conference* (pp. 2087-2091). IEEE.
- [62] Kharab, A., & Guenther, R. (2018). *An introduction to numerical methods: a MATLAB® approach*. CRC press.
- [63] Trinasolar. (2019). *The tallmax framed 72-cell module*. Site name.
http://static.trinasolar.com/sites/default/files/PS-M-0328%20E%20Datasheet_Tallmax_US_Feb_2017_A.pdf
- [64] Orioli, A., & Di Gangi, A. (2019). A procedure to evaluate the seven parameters of the two-diode model for photovoltaic modules. *Renewable energy*, 139, 582-599.
- [65] National Renewable Energy Laboratory. (2018, February 18). U.S. Annual Solar GHI.
<https://www.nrel.gov/gis/assets/images/solar-annual-ghi-2018-usa-scale-01.jpg>
- [66] Solaredge. (2020). *60-Cell Monocrystalline PERC Panel with Integrated Power Optimizer for Australia*. Site name.
https://www.solaredge.com/sites/default/files/se_smart_module_monoperc_australia.pdf